

Effect of an Axially Offset Impeller on the Transient Physics of Asymmetric Flow in a Double-suction Centrifugal Fan

R. Liu, H. Yang, Y. Wei, and W. Zhang[†]

Zhejiang Key Laboratory of Multiflow and Fluid Machinery, Zhejiang Sci-Tech University, Hangzhou, Zhejiang 310018, China

[†]Correspondence author Email: zhangwei@zstu.edu.cn

ABSTRACT

The impeller of a double-suction centrifugal fan may be subject to axial offset due to assembly or operational failure. The internal flow is asymmetric about the central disc and deteriorates the fan's performance. In this work, the characteristics of flow were numerically investigated for the baseline model (Model-BM) and the axially offset impeller model (Model-Offset). The objective and motivation are to provide a detailed assessment and quantification of the effect of offset impeller on the fan's performance and transient physics of the asymmetric flow. The numerical data reveal that the offset impeller generates highly asymmetric flow. The difference in mean flow rate at the two inlets of Model-Offset is 25.02m³/h, accounting for 6.8% of the total flow rate. The static pressure rise reduces by 2.40% for Model-Offset, and the static pressure efficiency is reduced by 2.11%. The leakage flow gets pronounced in the enlarged clearance with the inward and outward motion of air, while the narrowed clearance blocks it. The reversed flow is significant in the NA-side blade passages, especially close to the impeller end ring, where the leakage flow and the volute tongue confinement dominate. The reversed flow persists throughout the impeller, is still evident as the air first enters the volute, and is significant on the NA-side of the fan outlet.

Article History

Received October 8, 2024
Revised February 17, 2025
Accepted February 18, 2025
Available online May 5, 2025

Keywords:

Double-suction centrifugal fan
Offset impeller
Asymmetric flow
Leakage flow
URANS

1. INTRODUCTION

The double-suction centrifugal fans are utilized for ventilation in many heating, ventilation and air-conditioning (HVAC) systems, considering their high-pressure rise and compact size advantages. The double-suction centrifugal fans consist of an impeller with multiple blades on two sides separated by the central disc, a volute, and two collectors to both sides, which direct the flow entering the fan. The fan performances are closely correlated with, if not entirely dependent on, the patterns of internal flow, which are governed by the geometrical features of the various components. For instance, the flow in the impeller is influenced by the axial clearance between the impeller's end ring and collector; a proper geometry and size of the clearance, such as that modified by a D-shaped collector (Liu et al., 2021), could reduce the reversed flow and improve the fan's performance. The radial clearance at the volute tongue is also a key parameter in the fan design.

The leakage flow in the axial clearance is crucial for the fan's performance since it degrades the working

capability of the impeller. A large clearance permits severe leakage and reduces the fan's efficiency, while a narrowed clearance prohibits the leakage flow and improves the fan's performance (Myung & Baek 1999; Lee, 2010). However, in practical applications, a tiny clearance leads to difficulty in installing the impeller within the volute. It may result in accidental collision between the impeller and the adjacent collector due to the failure after a long-term operation, thus degrading the fan's operational safety. Some works have investigated the effects of clearance size on the fan's performance. Lee (2010) observed the flow separation and downstream recirculation losses in a centrifugal fan due to an improper clearance size, which decreases 2%-5% of the fan efficiency. Lei et al. (2024) identified the severe leakage and highly unsteady internal flow induced by a large clearance in a centrifugal pump, intensifying the entropy production and consequently reducing hydraulic head and efficiency.

The aerodynamic or hydraulic matching of the various components of the centrifugal turbomachine affects the internal flow patterns. The relative position, including the different components' distance, orientation,

and alignment, determines the main and leakage flow characteristics. The effect of geometrical parameters of the double-suction centrifugal turbomachines has been examined. For a centrifugal pump, [Deng et al. \(2023\)](#) studied the energy dissipation and found that the flow structures strongly correlated with the hydraulic loss were identified by the Ω -vortex method and were found to be significantly impacted by the reversed flow; the main flow accounts for 54%-71% of the hydraulic loss. [Gangipamula et al. \(2022\)](#) examined the modification of vanes in a centrifugal pump. A novel trailing edge profile was proposed and achieves a 42% pressure pulsation reduction compared with the baseline model. However, an improper intermediate modification would instead intensify the vortex shedding and lead to higher pressure fluctuation. [Sonawat et al. \(2022\)](#) analyzed the pressure pulsation's effect on a centrifugal pump's hydraulic performance. The parametric investigation explored the impact of the stagger angle on the pulsation reduction and identified the optimal configuration of the impeller. The effectiveness of a split volute and a staggered impeller in mitigating the pressure pulsation was also evaluated. [Song et al. \(2019\)](#) studied the impact of blade stagger angle on a centrifugal pump's pressure fluctuation and internal flow. [Liu et al. \(2008\)](#) examined the impact of an inclined plain front disc in improving fan performance. [Chen et al. \(2024\)](#) explored the asymmetric flow induced by a three-dimensional inclined impeller of a centrifugal fan. The inclined impeller reduces the fan's efficiency, and the circumferentially non-uniform clearance intensifies the impeller's pressure fluctuation and flow separation. [Madhwesh et al. \(2018\)](#) optimized the size and position of the centrifugal impeller's circular end ring, improving fan efficiency. [Ye et al. \(2018\)](#) employed an oblique-cut design for the impeller blades to reduce the friction and blockage in the inlet duct of a centrifugal fan. The authors observed that the fan's efficiency and noise could be improved by imposing an appropriate axis displacement between the centers of the impeller and volute. [Chen et al. \(2022\)](#) examined the influence of the radially offsetting impeller in a centrifugal fan. The offset impeller leads to non-uniform static pressure distribution, the reversed flow, and the recirculation vortices in the blade passages. These factors adversely affect the volute's ability to diffuse the fluid. The impeller offsetting toward the baffle causes an increased reversed velocity, thus reducing the fan's efficiency. [Yang et al. \(2011\)](#) experimentally investigated the effect of relative displacement of the impeller and volute. The experiment revealed that the perfect alignment of the impeller and volute is not the optimal choice, while an appropriate shift could somewhat regulate the internal flow at the design condition, thereby improving efficiency and reducing noise.

For the centrifugal fans, the volute is designed to collect and guide the air towards the fan's outlet. The volute geometry determines the flow in the impeller primarily via the mechanisms of rotor-stator interaction, especially around the volute tongue, where the radial clearance is the smallest ([Zhou et al., 2018](#)). There were attempts to re-design or optimize the geometry of the volute to improve the performance and reduce the noise. [Samarbakhsh and Alinejad \(2011\)](#) optimized the openness

angle of the volute outlet. [Okauchi et al. \(2002\)](#) proposed four volute models of a centrifugal fan. The experiment confirmed the improved fan's performance at medium to high flow rates by the appropriate re-designed volute. [Li et al. \(2020\)](#) investigated the complex vortical structures and their formation near the volute outlet; the streamlines visualized the recirculation flow. [Pan et al. \(1999\)](#) modified the volute of the centrifugal fans and compressors and suggested an increased cross-section area near the volute tongue, which helps generate a uniform flow under off-design conditions. [Ding et al. \(2012\)](#) found that an increased volute openness improves the uniformity of flow but also results in more significant friction loss on the volute surface, leading to decreased fan efficiency. [Zhang et al. \(2016\)](#) found that for a centrifugal fan, the volute rather than the impeller primarily generates the noise, and the flow rate variation greatly influences the noise. [Younsi et al. \(2007\)](#) correlated the wall pressure fluctuation with the far-field acoustics of a centrifugal fan using the data of unsteady simulations.

It was concluded from the works, some of which were reviewed above, that the impeller-volute interaction generates pressure and velocity fluctuation and results in noise, which is the primary source for the centrifugal fans ([Wu et al., 2020](#)). The flow in the radial clearance affects the pressure fluctuation ([Jin et al., 2020](#); [González et al., 2006](#)). [Lv et al. \(2014\)](#) conducted numerical simulations to determine the optimal impeller position to improve the fan's efficiency. The optimized model reduces the leakage loss at the tongue and attenuates the pressure fluctuations. [Morinushi \(1987\)](#) studied the influence of volute tongue radius on the fan's outflow. The highest performance is achieved as the clearance is 8% of the impeller outlet diameter. [Rui et al. \(2020\)](#) investigated the impact of volute tongue radius on fan's performance. The enlarged clearance increases static pressure and weakens the reversed flow in the impeller. The impact of the clearance flow of a centrifugal blower was studied by [Patil et al. \(2018\)](#). The smaller clearance improves the fan performance by effectively reducing the recirculating flow near the volute tongue.

Although the low-speed industrial centrifugal fans, which contain only a few components, are geometrically simple compared with the compressors or turbines. However, the matching of the various components determines the fan's aerodynamic, aero-acoustic, and vibrational performances, making the fans a complex system. For the double-suction centrifugal fans, the atmosphere air enters the collectors on the two sides and exits from the single outlet of the fan; thus, there is intense flow interaction from the fan's two sides. The impeller is designed to be placed co-axially with the volute, and the central disc is right at the center of the volute to guarantee the best performance during operation. However, in practical applications, the impeller may be offset in the axial direction due to assembly error, loosening after a long-term operation, or inappropriate maintenance, which accidentally moves the impeller or volute. The imperfect positioning of the components would most likely degrade the fan's performance, even if the imperfection is minor.

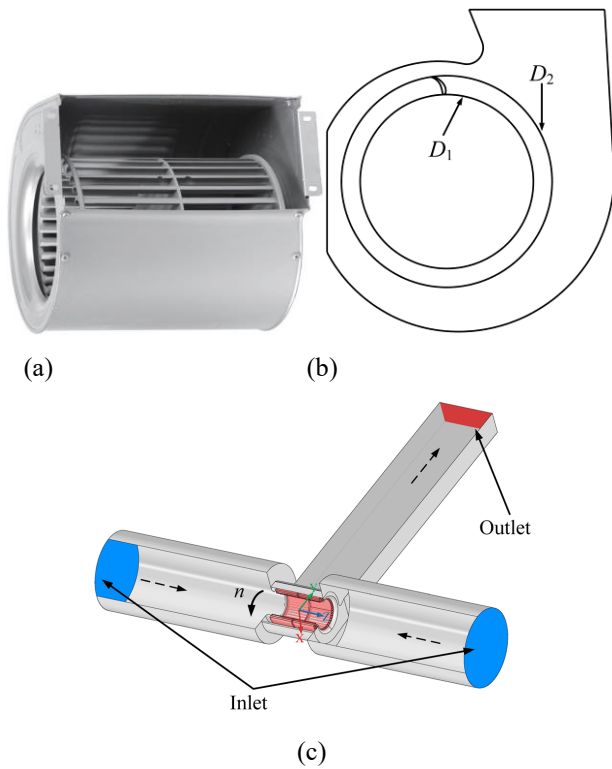


Fig. 1 Geometric model and computational domain: (a) the centrifugal fan; (b) the inlet (D_1) and outlet (D_2) diameter; (c) the computational domain including the centrifugal fan, the two enlarged inflow sections, and the outflow section

In most studies on flow in a double-suction centrifugal fan, the impeller is placed at a left-right symmetric position within the volute, and the possible axial offsetting of the impeller is usually ignored. The motivation and objective of this study are to consider the particular configuration of the impeller offsetting in the axial direction and perform a detailed assessment and quantification of its influence on the fan's performance. This work also focuses on the physics and mechanisms of the transient flow, emphasizing the asymmetric flow by comparing the characteristics in the two halves of the fan. The results, findings, and conclusions will provide a reference for research and applications in related fields. In terms of the flow physics and mechanisms, the transient flow in a double-suction centrifugal fan is revealed, with analysis on the flow asymmetry, the leakage flow in the axial clearance, the mean and unsteady behaviors of flow in the impeller, and the interaction and development of flow exiting from the two halves of the impeller. In engineering applications, the conclusions provide knowledge for future design, optimization, and assembly and maintenance of centrifugal fans or other double-suction centrifugal turbomachines. They are beneficial for related issues in engineering applications.

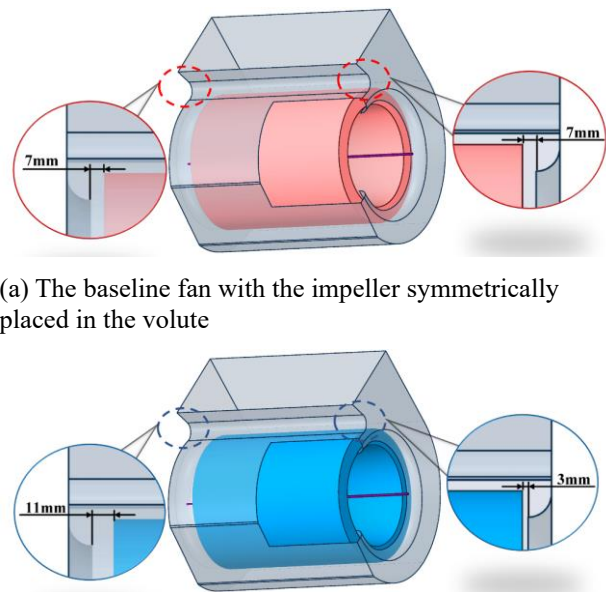
2. NUMERICAL DETAILS

2.1 Models of the Centrifugal Fan

A typical double-suction centrifugal fan with multiple forward-curved blades was chosen for this investigation.

Table 1 Parameters of the centrifugal fan

| Parameter | Value |
|--------------------------------------|-------|
| Flow rate, Q_n (m ³ /h) | 365 |
| Rotation speed of impeller (rpm) | 1200 |
| Impeller inner diameter, D_1 (mm) | 115 |
| Impeller outer diameter, D_2 (mm) | 140 |
| Volute width, B (mm) | 228 |
| Impeller width, b (mm) | 190 |
| Number of blades, N | 40 |



(a) The baseline fan with the impeller symmetrically placed in the volute

(b) The fan with the impeller axially offset in the volute

Fig. 2 Schematic of the fan models

The baseline fan model is shown in Fig. 1. The fan consists of the impeller, volute, and two collectors. An axial clearance between the impeller's end ring and the adjacent collector exists. Two inflow sections with enlarged cross-sections and an outflow section of a rectangular cross-section are introduced to permit the flow development to model the fan operating in a large space as in the experiment. The length of the inflow and outflow sections is five times that of the inlet and outlet diameter of the impeller, respectively, to avoid the reversed flow at the boundaries (Chen et al., 2022; Chen et al., 2024; Liu et al., 2024). The parameters of the fan are listed in Table 1.

The comparison between the fans with a symmetrically placed impeller and an axially offsetting impeller is given in Fig. 2. The impeller and volute are coaxially placed for the two models with unchanged geometry. For the baseline model (Model-BM), the impeller is placed in the volute in a left-right symmetric manner, and the distance between the impeller's end ring and the outlet cross-section of the adjacent collector is 7mm on both sides. For the fan with an offsetting impeller (Model-Offset), the impeller moves toward the right collector by 4mm, which accounts for only 2.86% of the impeller diameter (D_2) and 1.75% of the volute width (B);

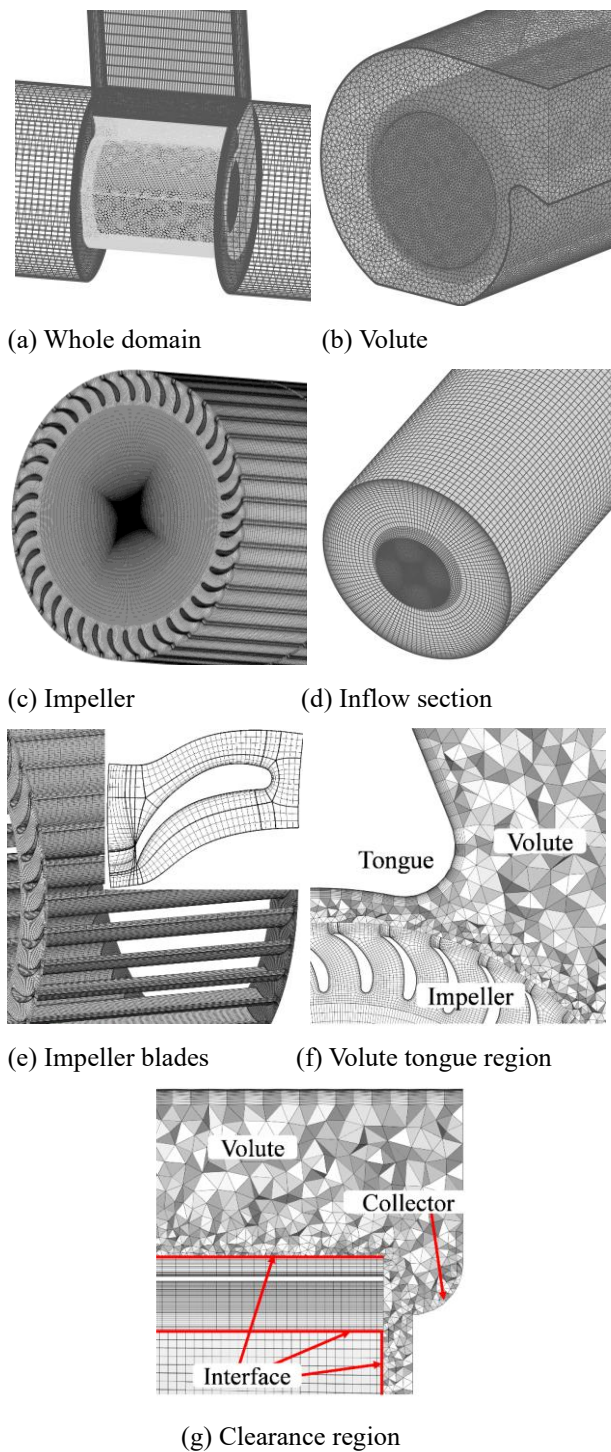


Fig. 3 Schematic of the grid

therefore, the distance becomes 3mm and 11mm in the two sides of the fan. To facilitate the following descriptions, the term PA-side (Positive-Axis) denotes the side where the impeller moves toward the collector, and the NA-side (Negative-Axis) represents the side where the impeller moves farther away from the collector.

2.2 Solution Method

The large-eddy simulation (Smagorinsky, 1963; Lilly, 1992; Versteeg and Malalasekera, 2007) (LES) method in ANSYS Fluent was employed for the simulation. A hybrid

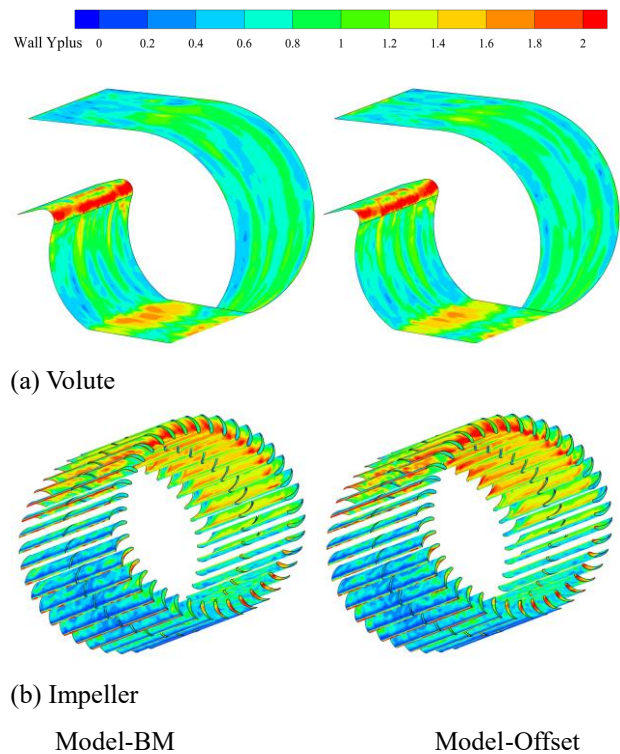


Fig. 4 Distribution of y^+ on the volute and impeller blades plotted using the instantaneous data obtained from the LES

grid was generated using ANSYS ICEM-CFD and Fluent Meshing, which is presented in Fig. 3. Due to their simple geometry, the hexahedral grid was used for the impeller and the inflow and outflow sections. The tetrahedral grid was used for the volute and rotor-stator interface. Most of the grids were allocated in the impeller and the volute. The grid was refined on solid walls. The height of the first layer grid is 0.005mm, and the extension ratio in the wall-normal direction is 1.3. The grid quality, as evaluated by ICEM-CFD, exceeds 0.3 over the whole computational domain. The minimum orthogonal quality is 0.36 for the impeller sub-domain. The distribution of y^+ on the blade and the volute is given in Fig. 4 as obtained from the instantaneous data; the maximum value of y^+ is 3.04 on the volute and 7.34 on the blade for Model-BM, while it is even slightly lower for Model-Offset.

The unsteady simulations were performed at the design flow rate of 365m³/h. The convective and viscous terms were spatially discretized using the second-order upwind and central difference schemes, respectively, and the temporal discretization was performed using the second-order implicit scheme. The constant flow rate was fixed at the outlet for the boundary conditions, and zero total pressure was prescribed at the inlet. The velocity follows no-slip conditions on the walls. The rotor-stator interface was set as a general connection in the software.

Since the LES is quite time-consuming, a time-efficient steady-state Reynolds-averaged Navier-Stokes (RANS) simulation was first performed to obtain an approximation of the flow rapidly. The converged solution was employed to initialize the subsequent production LES

Table 2 Details of the grid number

| Sub-domain | Number of grids ($\times 10^6$) |
|-------------------|-----------------------------------|
| Impeller | 4.21 |
| Volute | 1.80 |
| Inflow extension | 0.75 |
| Outflow extension | 0.36 |
| Total | 7.12 |

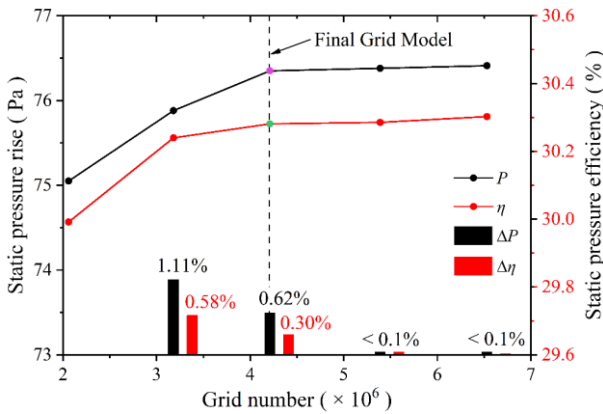
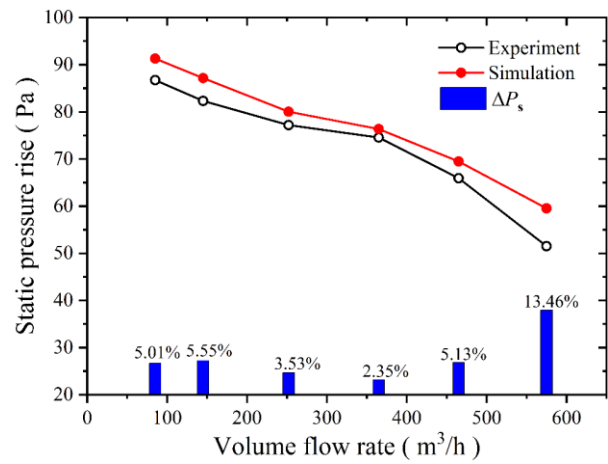


Fig. 5 Static pressure rise and efficiency obtained using different impeller grids. The columns denote the relative difference between the current grid and the next coarser grid

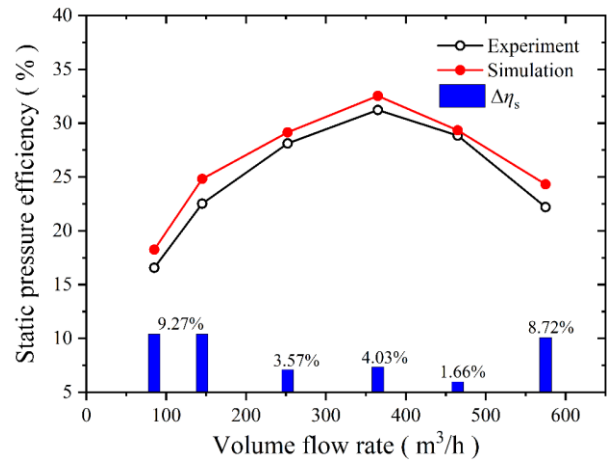
simulation. The time step size was fixed at 1.389×10^{-4} second, corresponding to a time interval as the impeller rotates for 1° as calculated from the rotation speed of 1200rpm, which is a common choice for different types of turbomachinery such as a centrifugal pump (Deng et al., 2003; He et al., 2025; Li, 2025), Pelton turbine (Lu et al., 2024) or axial fan (Sun et al., 2021). A total number of 20 inner iterations was set unless the relative residual reached a pre-defined value of 10^{-5} for each variable. The transient simulation first runs for 12 impeller revolutions to erase the existing effects of the approximated initial field, and the instantaneous data produced in the subsequent two revolutions was used for statistics.

2.3 Grid Sensitivity Study and Validation

A grid sensitivity study evaluated the sufficiency of the grid number in accurately resolving the transient flow in the fan. The number of grids of the impeller varies from 2.26 million to 6.53 million. In contrast, considering their comparably simple geometry, the number of grids for the volute, inflow, and outflow sections remained unchanged. The static pressure rise and efficiency of Model-BM computed using the grids are given in Fig. 5. Both pressure rise and efficiency approach constant as the number of grids increases. The relative difference between the two quantities between the set of 4.21 million grids and the next set with finer grids is less than 0.1%, indicating the sufficiency of the resolution. The set of grids with 4.21 million grids for the impeller sub-domain and 7.12 million grids for the whole computational domain was employed in all simulations. The grid details are given in Table 2.



(a) Static pressure rise



(b) Static pressure efficiency

Fig. 6 Numerical and experiment data, the columns denote the relative difference

The numerical data of Model-BM was validated against the experimental data obtained in the aerodynamic-aeroacoustic laboratory of Zhejiang Yilida Ventilator Co. Ltd. conforming to International Standard ISO5801-2007 and National Standard of China GB/T1236-2017. The uncertainty of the experimental data is around 1.1%, as certified by the China National Accreditation Service for Conformity Assessment (CNAS). See Rui et al. (2020) for the experimental details. Fig. 6 shows the data of static pressure rise and efficiency at various flow rates. The numerical data is generally consistent with the experimental data. At the design flow rate of $365 m^3/h$, as we investigated in this work, the relative difference is 2.35% and 4.03% for the two quantities. Therefore, we believe the numerical simulation reliably reflects the fan's performance.

3. RESULTS AND DISCUSSION

3.1 Aerodynamic Performances

The aerodynamic performances of the centrifugal fan considering the impeller offsetting are first analyzed since

Table 3 Aerodynamic performance quantities

| Parameter | Model-BM | Model-Offset |
|---|----------|--------------|
| Mean static pressure rise (Pa) | 83.25 | 81.25 |
| RMS static pressure rise (Pa) | 4.77 | 4.93 |
| Mean static pressure efficiency (%) | 36.98 | 36.20 |
| Mean flow rate, NA-side (m ³ /h) | 180.00 | 169.97 |
| Mean flow rate, PA-side (m ³ /h) | 185.05 | 194.99 |

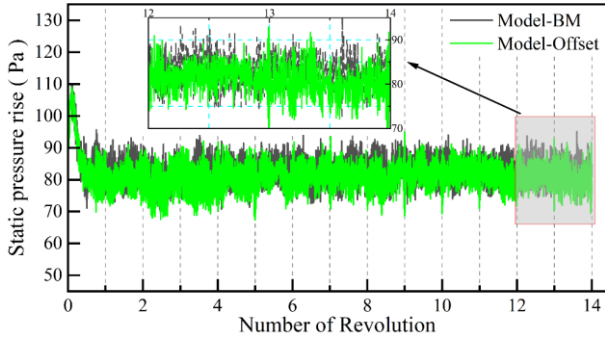


Fig. 7 Time history of static pressure rise

they are of particular interest to the users. The static pressure rise is the difference between the magnitude at the outlet and the average value at the two inlets. Fig. 7 shows the static pressure rise for 14 impeller revolutions, starting from the converged solution of the RANS simulation, as demonstrated above. For both fan models, the static pressure rise fluctuates around a constant value from the second revolution, justifying the decision based on the statistics of the computed data in the last two impeller revolutions. It is seen that the static pressure rise fluctuates roughly between 70Pa and 90Pa for both models, indicating that the offset impeller does not notably affect the fluctuation for the whole fan.

The time-averaged value and the root-mean-square (RMS) fluctuation of the characteristic quantities assess the influence of the impeller offsetting. The two quantities are defined as:

$$\langle f \rangle(\mathbf{x}) = \frac{1}{\Delta t} \int_0^{\Delta t} f(\mathbf{x}, t) dt \quad (1)$$

$$f_{\text{RMS}}(\mathbf{x}) = \sqrt{\frac{\int_0^{\Delta t} [f(\mathbf{x}, t) - \langle f \rangle(\mathbf{x})]^2 dt}{\Delta t}} \quad (2)$$

Table 3 lists the statistical quantities for the two models. The mean static pressure rise for Model-Offset is 2.40% lower than that of Model-BM, and the efficiency is 0.78% lower. Although the difference is minor, the decreased values reflect the noteworthy performance degradation induced by the impeller offsetting, which is undesired in engineering applications. The temporal fluctuation of static pressure rise increases by about 3% for Model-Offset. The slightly larger fluctuation represents the stronger unsteadiness of the internal flow due to the impeller offsetting. Referring to Fig. 7, the fluctuation of static pressure rise of Model-Offset exhibits a low-frequency modulation in addition to the high-

frequency one induced by the periodic passing of multiple blades. The more significant fluctuation is attributed to the instantaneous value that deviated from the time-averaged value.

The offset impeller is closer to the PA-side collector than the NA-side collector; thus, the amount of air entering the fan through the two collectors differs. The constant total pressure was set at the inlet to permit the full development of incoming air and adapt it to the fan's geometry. The mean flow rate is calculated at the two inlets of the fan, specifically at the inlet of the collectors, to quantify the influence of impeller offsetting. It is seen that there is a minor difference of 5.05m³/h at the two inlets of Model-BM. The non-zero difference is due to the inherent bifurcation arising from modeling the complex geometry of the centrifugal fan; it is first zero as the simulation starts, then gradually increases and is around a constant value. For Model-Offset, the impeller-collector interaction affects the inflow, which presents different flow rates at the two inlets. The difference is 25.02m³/h, approximately four times larger than that of Model-BM. The impeller offset toward the PA-side collector reduces the axial clearance, thus imposing centrifugal force on the inflow more efficiently, strongly driving the incoming air entering and exiting the fan. The axial clearance in the NA-side of the fan is enlarged and intensifies the leakage flow, which is a source of the fan performance degradation.

In summary, the axial offsetting impeller decreases the static pressure rise and efficiency. It also slightly destabilizes the internal flow, generating a higher pressure fluctuation. The narrowed PA-side axial clearance increases the local volume flow rate while decreasing the NA-side flow rate of the centrifugal fan.

3.2 Flow in the Collector

It is discussed above that the mean flow rate at the two inlets of the fan is different as affected by the axially offsetting impeller. Since the atmosphere air entering the centrifugal fan first moves through the two collectors, the flow field in the collectors is analyzed in this section. Considering that the collector has a converging geometry toward the fan interior, and its outlet is the closest to the impeller, the mean static pressure field at the collector outlet is given in Fig. 8. The magnitude of static pressure is generally high in the central region of the cross-section for both models. It gradually decreases and reaches a minimum at the edge, i.e., the collector's surface. The low-pressure results from the accelerated air, which is collected from the atmosphere and enters the collectors attaching to the surface. However, the incoming air is not accelerated by any obstruction in the central cross-section;

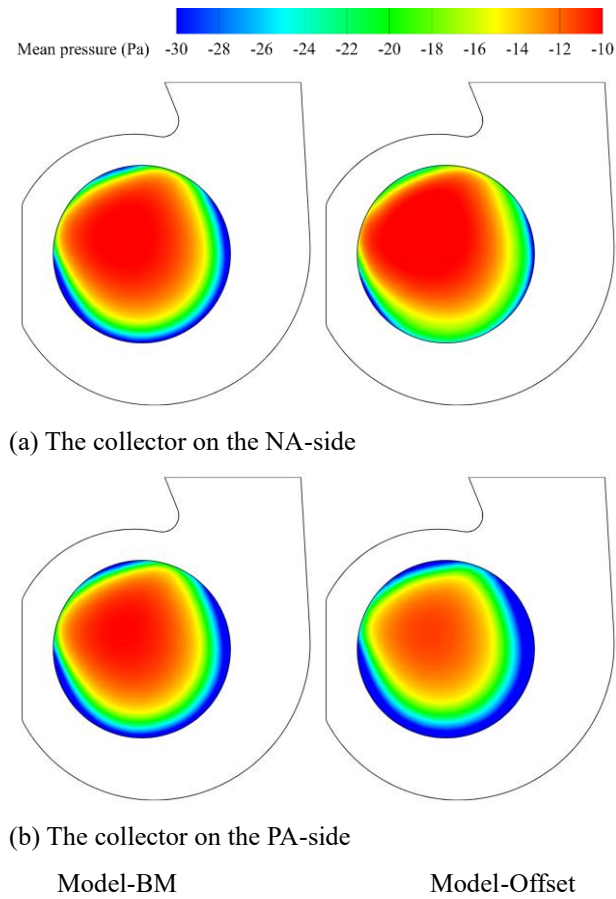


Fig. 8 Mean static pressure field at the collector's outlet

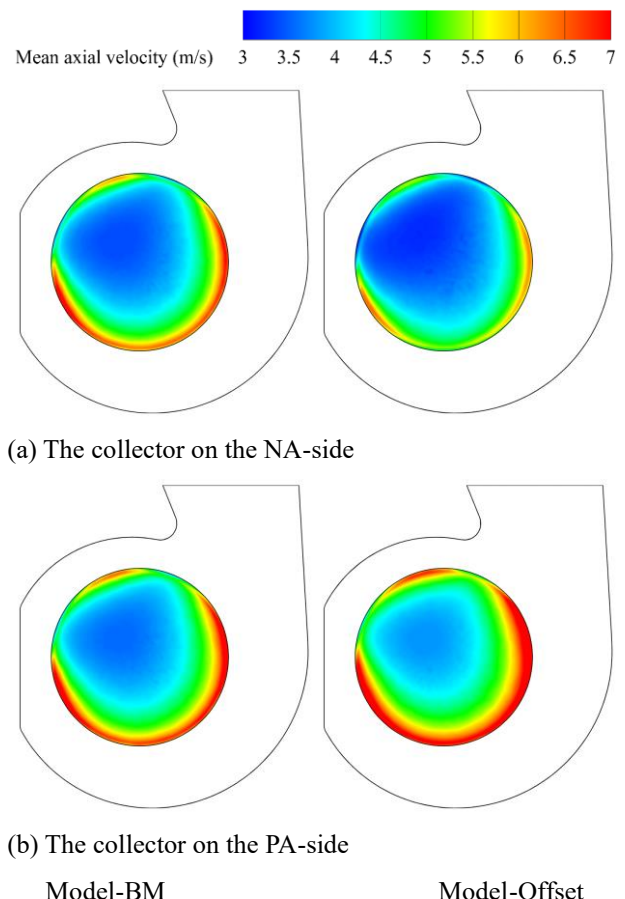


Fig. 9 Mean axial velocity field at the collector's outlet

thus, the static pressure is generally high. The offset impeller varies the static pressure field, making the distribution asymmetric in both collectors. Compared with Model-BM, the high-pressure region in the NA-side collector of Model-Offset enlarges in size; the magnitude reaches around -20Pa for the majority edge region, i.e., close to the collector surface. On the contrary, in the near-wall region of the PA-side collector, the static pressure significantly decreases in magnitude, forming a ring-type low-pressure region close to the collector surface for almost the whole circumference; the high-pressure in the central cross-section also reduces in size and magnitude.

The static pressure variation at the collector outlet is correlated with the inflow patterns. Since constant total pressure is set for the inflow, the static pressure and dynamic pressure vary in opposite trends. Fig. 9 presents the field of mean axial velocity at the outlet cross-section; the positive value denotes the air moving toward the fan interior. It is seen that the velocity magnitude is low in the central cross-section but notably high close to the collector surface, showing a distribution that is contrary to that of static pressure, as given in Fig. 8. The contrary distribution pattern is attributed to the incoming air's constant mechanical energy, which is not yet affected by the impeller rotation at this cross-section; the air moving over the curved surface of the collectors experiences the streamline curvature and is accelerated at

the expense of reduced static pressure. By comparing the velocity field of Model-BM and Model-Offset, it is seen that the offset impeller influences the magnitude of velocity, but not the distribution pattern, in the regions at the center and the boundary of the two collectors. For the inflow in the NA-side collector, the axial velocity is significantly decreased in magnitude over the whole cross-section, resulting in the reduced flow rate as listed in Table 3; the decreased axial velocity is believed to be a consequence of the reduced driving force on the incoming air provided by the impeller. However, the inflow in the PA-side collector increases in axial velocity due to the approaching of the impeller; the increased axial velocity is the most pronounced near the collector's wall. Moreover, it is noticed in Fig. 8 and Fig. 9 that the pressure and velocity do not exhibit concentric-like distributions; the region with high pressure and low velocity is biased toward the volute tongue and its downstream region for both models. The low magnitude of axial velocity around the volute tongue results from the volute confinement, which partially blocks the outflow of the impeller; thus, the inflow is also blocked.

The circumferential non-uniform axial velocity field is further quantitatively analyzed using the velocity distribution on the two straight lines. Fig. 10 presents the positions of the two lines; Line-I is along the X-direction from the bottom to the top of the fan, and Line-

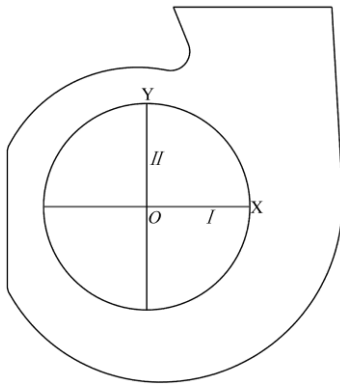


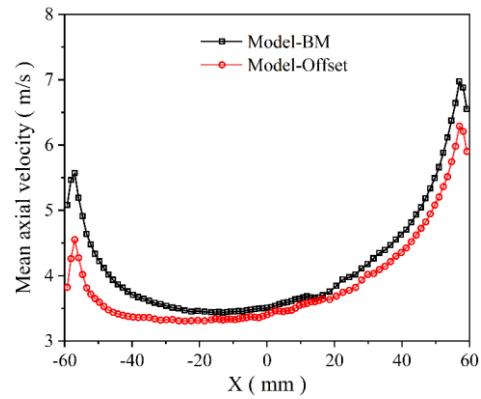
Fig. 10 Definitions of Line-I and Line-II at the outlet cross-section of the two collectors.

II is along the Y-direction. The distribution of axial velocity is given in Fig. 11 for the two models. In general, the velocity profile of Model-BM is quite similar for the inflow at the two collectors. However, there is still a minor discrepancy considering the inherent asymmetry of the inflow. For Model-Offset, the velocity profile differs depending on the side of the collector. By comparing Fig. 11a and Fig. 11c, it is found that the distribution of velocity magnitude at Line-I of the two collectors is also different except for the larger velocity magnitude for flow in the PA-side collector. The magnitude is larger for flow moving over the right side of the collector ($X \rightarrow 60\text{mm}$) in the NA-side collector but for the left side ($X \rightarrow -60\text{mm}$) in the PA-side collector. Considering that the axial velocity is always higher in magnitude in the PA-side collector for Model-BM, the discrepancy between the axial velocity of inflow of Model-Offset is a reflection of the circumferentially varied influence of the offset impeller. The finding is confirmed by the comparison of the velocity profile on Line-II, as given in Fig. 11b and Fig. 11d; the velocity of Model-Offset differs mainly in magnitude, while the distribution pattern is almost identical. The quantitative comparison reflects the influence of impeller offsetting via the approaching of the impeller toward the PA-side collector.

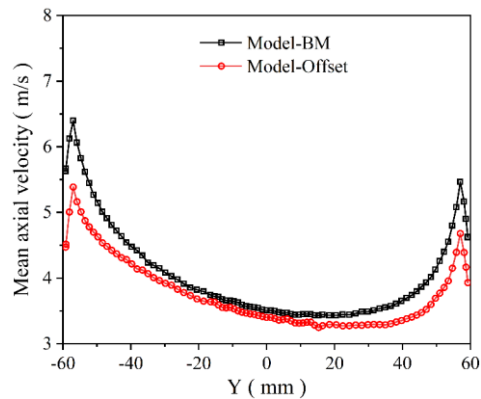
In summary, the offset impeller increases the mean static pressure. It reduces the mean axial velocity in the NA-side collector from which the impeller moves away. In contrast, the opposite variation trend of the static pressure and axial velocity is observed for the PA-side collector from which the impeller approaches. The separated impeller and collector weaken the capability of the impeller to drive the atmosphere air entering the fan.

3.3 Leakage Flow in the Axial Clearance

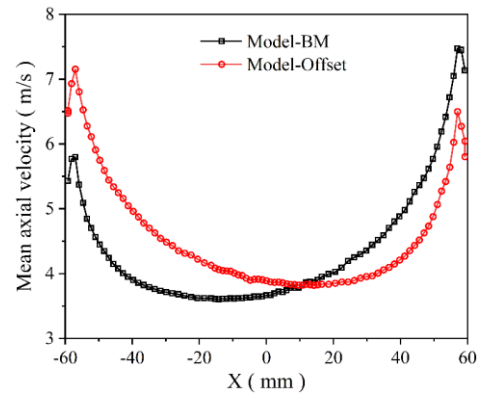
There is leakage flow in the axial clearance due to recirculating flow, which wastes the input energy and deteriorates the fan's performance. The axial clearance permits the incoming air to move in the radial direction before entering the impeller's central region. Since the axial clearance is small and is connected with the fluid domain of the impeller (see Fig. 2), the leakage flow at another position, i.e., the clearance between the impeller end ring



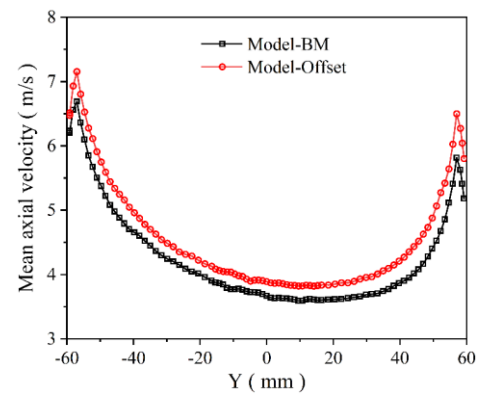
(a) Line-I for the NA-side collector



(b) Line-II for the NA-side collector



(c) Line-I for the PA-side collector



(d) Line-II for the PA-side collector

Fig. 11 Mean axial velocity distribution along Line-I and Line-II at the collector outlet

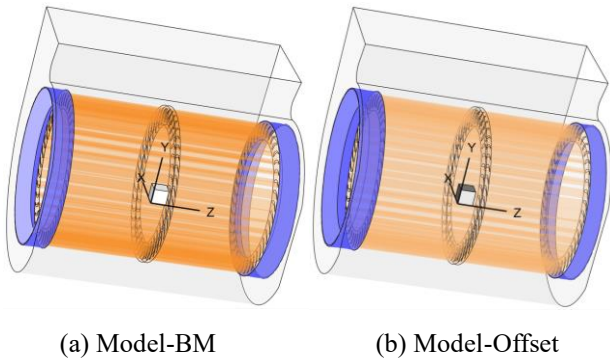


Fig. 12 Definition of the clearance at R=72mm between the impeller and collector

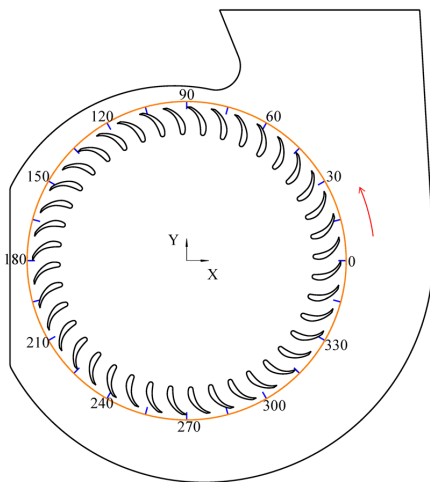


Fig. 13 Definition of the circumferential coordinate for the impeller

and the volute, as shown in Fig. 12, is analyzed. This clearance is defined approximately at the impeller outlet’s radial position, and the figure indicates the revolution surface. The incoming air leaked from the collector will primarily move through the axial clearance. The area of the two clearances is the same for Model-BM but is not for Model-Offset. The circumferential direction for the two fan models is shown in Fig. 13. The circumferential coordinate is counterclockwise, and the circumferential position of 0° is in the positive X-direction.

Since the axial clearance is geometrically a surface of revolution, the flow leaked from the clearance is quantified by the local radial velocity perpendicular to the surface. Fig. 14 presents the mean radial velocity distribution at the clearance of each model. The radial velocity with a positive magnitude indicates the outward moving fluid, i.e., from the collector/impeller to the volute. There is a recirculating flow in the clearance, i.e., the air moves outward and inward through the clearance at different circumferential regions. The air moves outward through the clearance primarily at 90°-240°, while the inward motion occurs in the rest of the clearance. The inward motion of

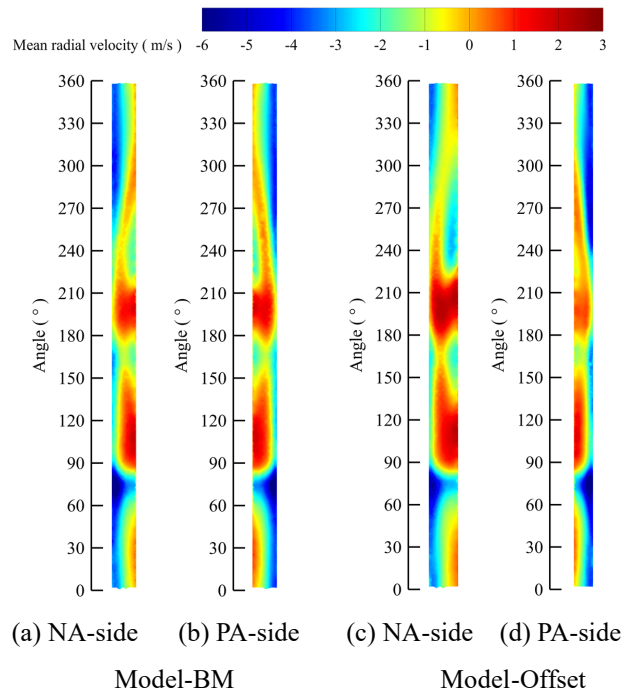


Fig. 14 Mean radial velocity field on the R=72mm cross-section

air, with negative radial velocity, appears at the volute surface where local air is weakly driven by the impeller; it is driven by the pressure gradient since the pressure in the volute is higher than that in the clearance. The inward flow motion is also substantial at 60°-90°, i.e., around the volute tongue, where the clearance is almost entirely occupied by the inward moving air, which results from the wall confinement of the adjacent volute surface.

A comparison of the radial velocity field for Model-BM and Model-Offset shows that the offset impeller does not affect the general patterns of radial velocity distribution; the air’s outward and inward motion still occur at the same circumferential regions. Due to the enlarged clearance in the NA-side of the fan, the outward motion of air through the clearance in the region 90°-240° is intensified in both magnitude and area of the positive radial velocity, and the inward moving air in the region 270°-360° is significantly weakened. The pronounced difference, especially for the outward-moving air, indicates that the enlarged clearance weakens the radial pressure gradient; the radial motion of air is primarily driven by the inertia but not the weakened pressure gradient. In the PA-side of the fan, where the clearance is narrowed, the outward-moving leakage flow gets weakened compared with Model-BM, while the inward flow is unaffected. This observation implies that the narrowed clearance mainly prohibits the outward motion of air but not the inward motion, indicating a superior impact from the radial pressure gradient than the fluid inertia.

The radial velocity field in the clearance demonstrates that the leakage flow is determined by the intensity of fluid inertia and the radial pressure gradient. In the NA-side of Model-Offset, where the clearance is

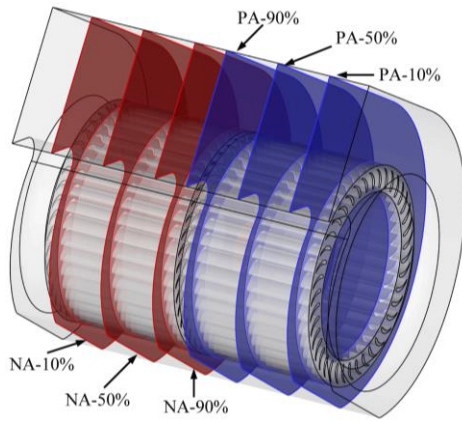


Fig. 15 Definition of constant-Z cross-sections in the fan

enlarged, the pressure gradient is weakened; thus, the inertial-driven outward motion of air occupies the clearance. On the contrary, in the narrowed PA-side clearance, the fluid inertia could not resist the pressure gradient; thus, the local flow mainly presents an inward motion on the volute surface, and the outward moving air notably reduces in velocity magnitude and area. An exception is the region at the volute tongue, where the volute confinement generates the persistent inward motion of air, and the velocity magnitude and area of the inward-moving air do not vary much as the clearance size changes.

3.4 General characteristics of flow in the fan

The incoming air entering the fan through the collectors moves through the impeller blade passages and is collected in the volute. The internal flow directly determines the fan's performance. The instantaneous static pressure and streamline field are presented to analyze the general characteristics of asymmetric flow. The flow field is exhibited on several constant-Z cross-sections in the two halves of the fan, which are placed close to the central disc (PA-90% and NA-90%), in the middle of the impeller (PA-50% and NA-50%), and close to the collector (PA-10% and NA-10%), respectively, as shown in Fig. 15.

The static pressure and streamline field on the various cross-sections are presented in Fig. 16 and Fig. 17 for the NA-side and PA-side, respectively. The magnitude of static pressure is the lowest in the central impeller where the incoming air first enters the fan; it increases in the blade passages as driven by the impeller and is generally the highest in the volute due to pressure recovery. The magnitude also depends on the cross-section's position. It is low as the air first enters the fan, i.e., on the NA/PA-10% cross-sections, since the local inflow moves in the axial direction and is not yet effectively driven by the impeller. The magnitude increases as the air moves toward the central disc; the increasing static pressure is observed over the whole cross-section, especially in the impeller. The increased pressure is associated with the transition of the direction of the air as it moves in the radial direction

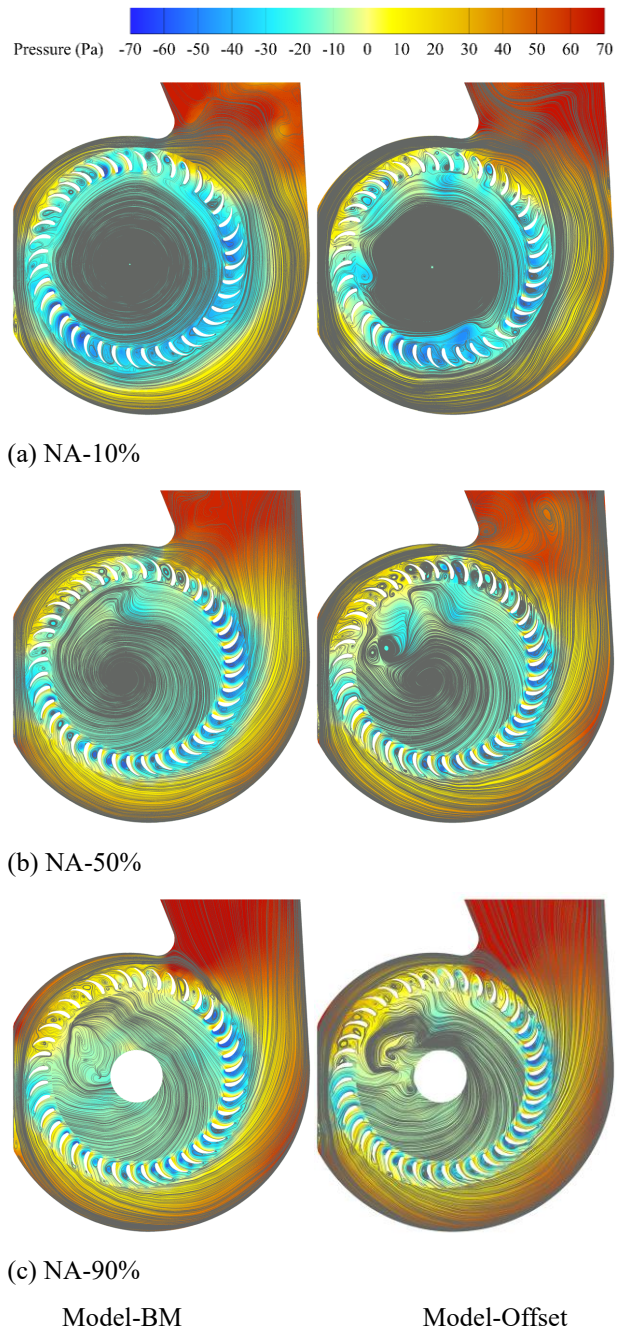


Fig. 16 Field of the instantaneous static pressure and streamlines on the NA-side cross-sections of the impeller, which moves away from the adjacent collector

through the blade passages; thus, the kinetic energy transferred to the air by the impeller begins to convert to static pressure.

The influence of impeller offsetting is revealed by comparing the flow field of Model-BM and Model-Offset. In the entrance region, i.e., the NA/PA-10% cross-sections, the recirculating vortices are formed in multiple blade passages for both fan models. However, the size, distribution, and number of vortices differ. On the NA-10% cross-section, the recirculating flow is generated in almost all blade passages. The recirculating vortices are the most

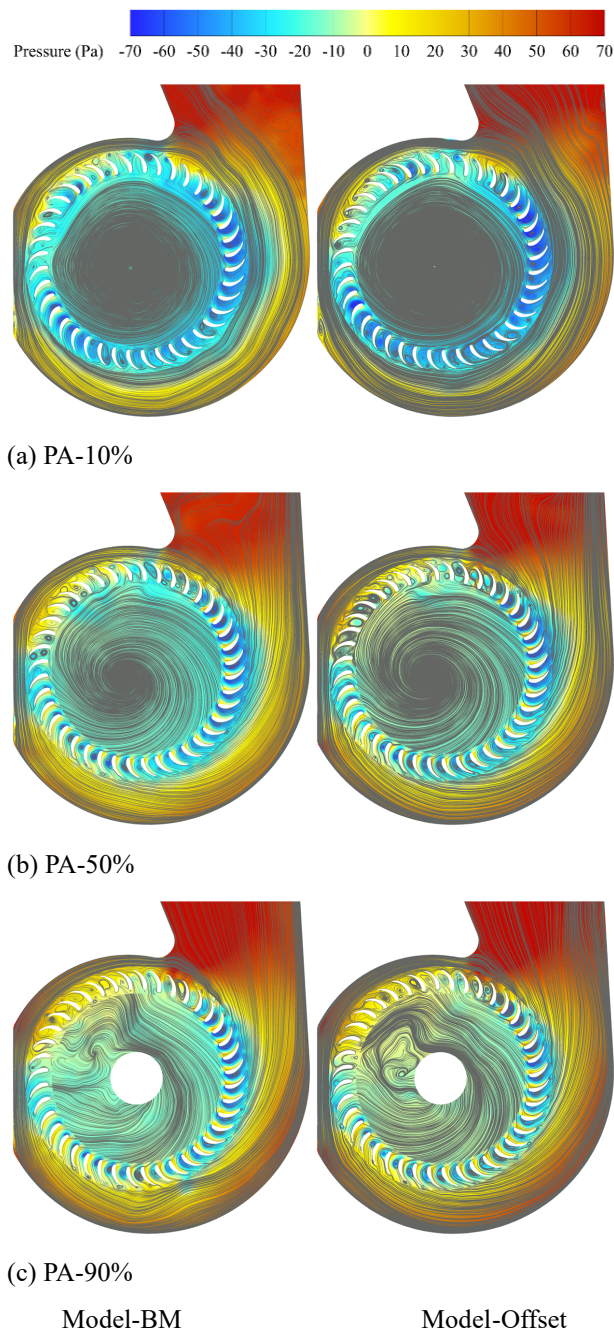


Fig. 17 The field of the instantaneous static pressure and streamlines on the PA-side cross-sections of the impeller, which moves away from the adjacent collector

notable for the blade passages at 225° - 360° (see Fig. 13 for the definition of the angular coordinate) and at 90° - 150° where the vortices almost fully occupy the blade passages. The recirculating vortices in the blade passages of Model-BM are comparably smaller in size, but the difference is not apparent. The static pressure for Model-Offset shows a circumferentially non-uniform distribution in the blade passages; the static pressure is the highest at 90° - 180° and in those around 60° and 225° but is comparably lower in the rest of the blade passages. The lowest magnitude appears in the blade passages around 340° . The non-monotonic variation of static pressure in

the circumferential direction is not evident for Model-BM; the static pressure is higher around the volute tongue and is low in the rest of the blade passages. The distribution of the PA-10% cross-section is similar for Model-BM and Model-Offset. The instantaneous field indicates that the flow in the NA-side entrance region (NA-10% cross-section) is strongly affected by the offset impeller due to the enlarged clearance. In contrast, the narrowed clearance on the PA-side has a minor influence on flow in the blade passages.

The flow on the NA/PA-50% and NA/PA-90% cross-sections is not significantly affected by the impeller offsetting since it is away from the collectors where the axial clearance varies in size. The static pressure field is quite similar for the two models; the non-monotonic variation, i.e., with a better pressure recovery in the blade passage around 225° , is observed for both models. On the NA-50% cross-section, the magnitude of static pressure at 90° - 180° increases for Model-Offset and is higher than that of Model-BM, while it almost does not change for other blade passages. The increase in static pressure is inapparent on the NA-90% cross-section since it is far from the axial clearance. The narrowed axial clearance has weak impact on flow on the PA-50% and PA-90% cross-sections, as presented by the almost identical pressure distribution. However, the recirculating vortices almost diminish in the blade passages at 90° - 180° on the PA-90% cross-section of Model-BM, while they are still observed for Model-Offset.

It is summarized that the offset impeller notably impacts the flow close to the collectors, and the impact is more pronounced for the NA-side of the fan where the clearance is enlarged. The static pressure in the blade passages around the volute tongue increases in magnitude; thus, static pressure distribution becomes circumferentially non-monotonic. The flow on the NA/PA-50% and NA/PA-90% cross-sections is less affected by the impeller offsetting; the static pressure and streamline field is similar for the two models, especially in the PA-side of the fan.

3.5 Flow in the Blade Passages: Mean Velocity

The recirculating vortices in the impeller present circumferentially non-uniform distribution and are different on the various cross-sections. The flow development in the impeller is affected by the volute through the mechanism of wall confinement, the curved blade surfaces, and the axial clearance where leakage flow forms. Three constant-R cross-sections are defined at the inlet ($R=59\text{mm}$), middle ($R=64\text{mm}$), and outlet ($R=69\text{mm}$) of the blade passages, as given in Fig. 18. The instantaneous radial velocity is calculated on the intersecting line of a constant-R cross-section and a constant-Z cross-section (NA/PA-10%, 50%, 90%). The positive and negative radial velocity in the blade passages is roughly considered forward flow and reversed flow, respectively. The mean radial velocity distribution in the multiple blade passages is shown in Fig. 19-Fig. 21 at various radial positions. The disconnections in the curve result from the blades of finite thickness. The difference

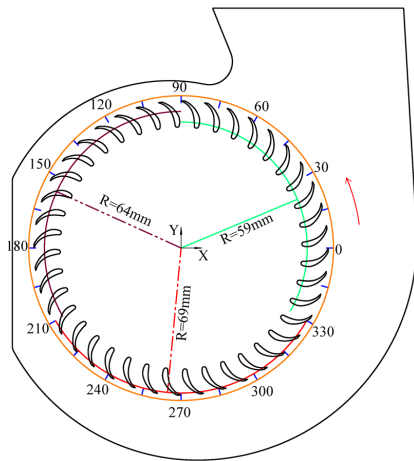


Fig. 18 Constant- R cross-sections at the inlet ($R=59\text{mm}$), middle ($R=64\text{mm}$), and outlet ($R=69\text{mm}$) of the blade passages

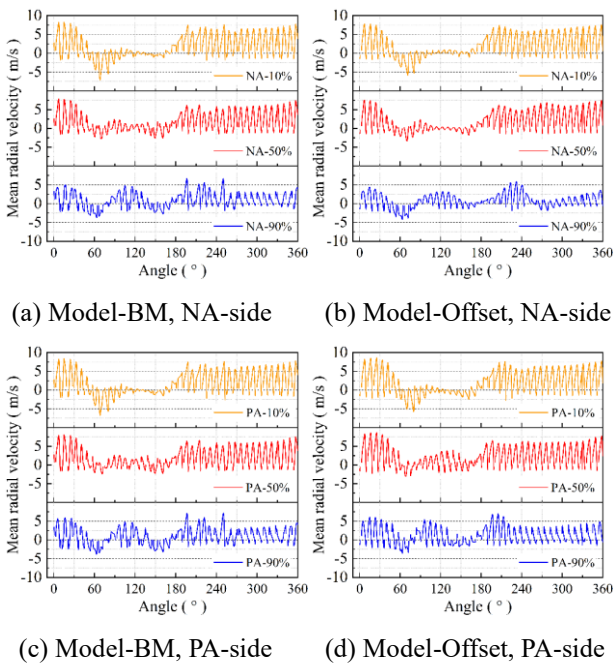


Fig. 19 Mean radial velocity distribution at the inlet of the blade passages ($R=59\text{mm}$)

among the curves in each sub-figure denotes the variation of the flow patterns in the same blade passage, and the difference between the curves in different sub-figures reflects the impact of the impeller offsetting.

The mean radial velocity distribution at the inlet of the blade passages ($R=59\text{mm}$) is presented in Fig. 19. For Model-BM, the velocity distribution is almost identical in magnitude and variation in each blade passage for the two symmetric cross-sections about the central disc. Although the flow rate is slightly different at the two inlets, as shown in Table 3, the identical distribution reflects that the flow in the impeller interior is unaffected due to the intense driving of the impeller even at the inlet. The reversed flow is substantial around the circumferential position of 70° ,

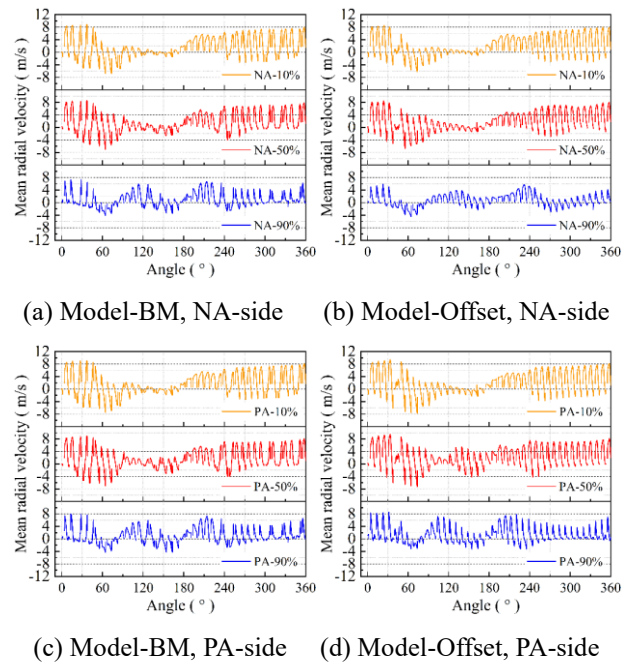


Fig. 20 The mean radial velocity distribution at the middle of the blade passages ($R=64\text{mm}$)

i.e., the volute tongue, due to the wall confinement that large-scale recirculating vortices form in the blade passage, as exemplified in Fig. 16 and Fig. 17. The reversed flow has the most remarkable magnitude at the NA/PA-10% cross-sections, where the incoming air first enters the fan and subjects to an abrupt transition from axial to radial direction. The direction transition reduces the kinetic energy for the air moving in the radial direction; thus, it is difficult for the air to resist the adverse pressure gradient. The weak reversed flow also forms at 105° - 165° , especially for the flow on the NA/PA-50% and NA/PA-90% cross-sections, whose peak magnitude is comparable to the reversed flow around the volute tongue. The reversed flow is attributed to a strong adverse pressure gradient field, as seen in Fig. 16 and Fig. 17. The distribution of mean radial velocity for Model-Offset is similar to that of Model-BM. The comparison of the distribution on the two sides shows that the forward flow in the PA-side has a larger velocity magnitude on all three cross-sections, especially for the PA-90% cross-section; the magnitude is more significant than that of the NA-90% cross-section for the whole circumference. Considering that the flow rate on the PA-side is higher, as listed in Table 3, the different velocity magnitude shown in this figure indicates that the increased flow rate is mainly contributed by the flow moving through the blade passages in the middle of the impeller and near the central disc. In contrast, the flow near the end ring almost negligibly contributes. The reversed flow downstream of the volute tongue at 105° - 165° is observed on both sides of the fan. It is weak in magnitude, and the difference between the flow on the two sides is inapparent.

The mean radial velocity distribution at the middle blade passages ($R=64\text{mm}$) is given in Fig. 20. The reversed flow around the volute tongue of Model-BM

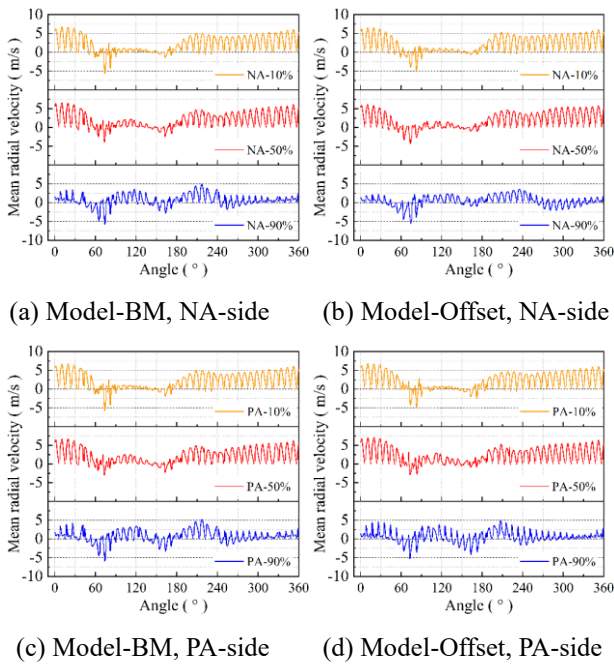


Fig. 21 The mean radial velocity distribution at the outlet of the blade passages (R=69mm)

exists, while it is also notably observed in the blade passages at 0° - 60° and 240° - 360° , especially on the NA/PA-10% cross-sections near the fan inlet. The reversed flow corresponds to the multiple recirculating vortices. The non-uniformity, as reflected by the peak-valley amplitude of radial velocity, gets stronger compared with the flow at $R=59\text{mm}$. The intense non-uniformity reflected by the velocity distribution originates from the recirculating vortices in the blade passages, which exhibit forward and reversed motion at $R=64\text{mm}$. Moreover, it is seen in Fig. 16 and Fig. 17 that the recirculating flow fully occupies some blade passages while others are free from it. The occasional generation and vanishment of the recirculating flow at the middle blade passages produce the non-uniform circumferential distribution. Compared with Model-BM, the radial velocity in each blade passage is more uniform for Model-Offset. The velocity magnitude presents a smooth increase and decrease in each blade passage, rather than the drastic and unpredictable variation as Model-BM, for example, the distribution on the NA-90% cross-section. This observation indicates a much more regularized flow, although with recirculating vortices, forms in the blade passages of Model-Offset. The velocity distribution is different on the two sides of the impeller; the flow on the NA-side is more uniform in terms of the peak-valley difference of velocity magnitude in each blade passage and several neighboring blade passages. Considering that the forward and reversed flow originates from the recirculating vortices, the slight peak-valley difference represents the weak recirculation in the NA-side blade passages.

Fig. 21 shows the mean radial velocity at the impeller outlet ($R=69\text{mm}$). The local air mainly moves in the radial direction. The reversed flow still exists around the volute

tongue at 60° and close to the volute bottom at around 160° , which is induced by the wall confinement by the volute surface. For Model-BM, the reversed flow on the NA/PA-10% and NA/PA-50% cross-sections is pronounced around the volute tongue, while the magnitude reduces over the whole impeller circumference on the NA/PA-90% cross-sections. Therefore, the forward motion of air is weak, and minor reversed flow is generated at the outlet of five blade passages at 240° - 280° . The viscous effect of the central disc decelerates the air on the NA/PA-90% cross-sections. For Model-Offset, the mean radial velocity on the NA/PA-10% and NA/PA-50% cross-sections is quite close to that of Model-BM, with reversed flow near the volute tongue. The offset impeller noticeably affects the radial velocity on the NA/PA-90% cross-sections. It varies more significantly in the circumferential direction, and the peak magnitude for the forward and reversed flow is higher for the PA-side impeller. Considering that the NA/PA-90% cross-sections are far from the axial clearance, the radial velocity difference correlates with the varied local flow rate due to impeller offsetting. As shown in Fig. 19, the radial velocity is primarily positive at the impeller's inlet on both the NA/PA-90% cross-sections, and the magnitude is more prominent on the PA-side. However, the magnitude is slightly positive at the impeller outlet on both cross-sections, and a strong local reversed flow also forms, as shown in Fig. 21. The reduced radial velocity and intensified reversed flow demonstrate that at the impeller outlet at the NA/PA-90% cross-sections, a portion of the air entering the blade passage moves in the axial direction and exits from the impeller on other cross-sections, rather than the two at the NA/PA-90% positions; thus, there is a notable difference of velocity magnitude.

The velocity distribution presented in Fig. 19-Fig. 21 confirms the noticeable reversed flow due to volute tongue confinement. The radial velocity exhibits quite a different distribution in the NA-side and PA-side impeller. The distribution on each side is more uniform for Model-Offset. The impeller outflow is affected by the impeller offsetting mainly on the NA/PA-90% cross-sections; the air in the blade passages moves along the axial direction, producing weakened radial motion at the outlet.

3.6 Flow in the Blade Passages: Fluctuating Velocity

The interaction between stationary and rotational components destabilizes the flow in the fan. The flow fluctuation is represented by the RMS value of fluctuating radial velocity, and the distribution is presented in Fig. 22-Fig. 24 for flow at the inlet, middle, and outlet of the blade passages. The RMS value is always greater than zero, and a large magnitude represents the strong temporal fluctuation of the local flow, which appears at the central blade passage.

At the inlet ($R=59\text{mm}$), the fluctuation in the NA-side and PA-side impeller is quite similar for Model-BM. There are several peak fluctuations in the blade passages at 180° - 270° on the NA/PA-10% and NA/PA-50% cross-sections. By referring to Fig. 16 and Fig. 17, it is seen that these blade passages are free of the recirculating vortices

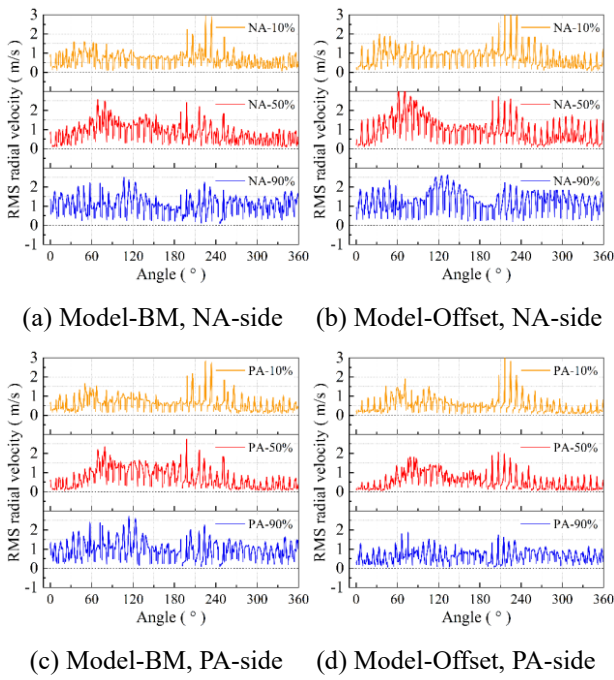


Fig. 22 The distribution of the RMS value of the radial velocity at the inlet of the blade passages (R=59mm)

or are occupied by small vortices compared with other blade passages. Therefore, as the blade passage moves into or away from this region, the internal flow subjects to the generation and vanishment of the vortices, thus presenting a remarkable fluctuation. However, as the blade passage moves to other regions, the recirculating vortices form within it and persist with the impeller rotation, which governs and stabilizes the flow, except for the notable effect of the volute tongue at 60°-90° that the fluctuation gets strong, especially on the NA/PA-50% cross-sections. For Model-Offset, the offset impeller intensifies the flow fluctuation on all three cross-sections on the NA-side of the impeller, and the intensification is significant for almost the whole circumference. The peak fluctuation at 180°-270° on the NA-10% and NA-50% cross-sections occurs in several neighboring blade passages rather than the discrete ones for Model-BM. Moreover, the highly fluctuating flow also appears roughly at 30°-60°, 60°-90°, and 100°-130° for the NA-10%, NA-50%, and NA-90% cross-sections, respectively, whose amplitude is more significant than that of Model-BM and other blade passages. The recirculating vortices formed at the inlet induce the local strongly fluctuating flow, as seen in Fig. 16. The recirculating vortices at the inlet might be as small as those on the NA-10% cross-section, or are the secondary vortices upstream of the primary ones, as those on the NA-50% and NA-90% cross-sections. The secondary vortices are subject to the periodic entrainment of the circulating flow in the impeller's central interior, producing more substantial perturbation. Compared with Model-BM, the fluctuating amplitude is substantially reduced on the PA-50% and PA-90% cross-sections for flow in the PA-side impeller.

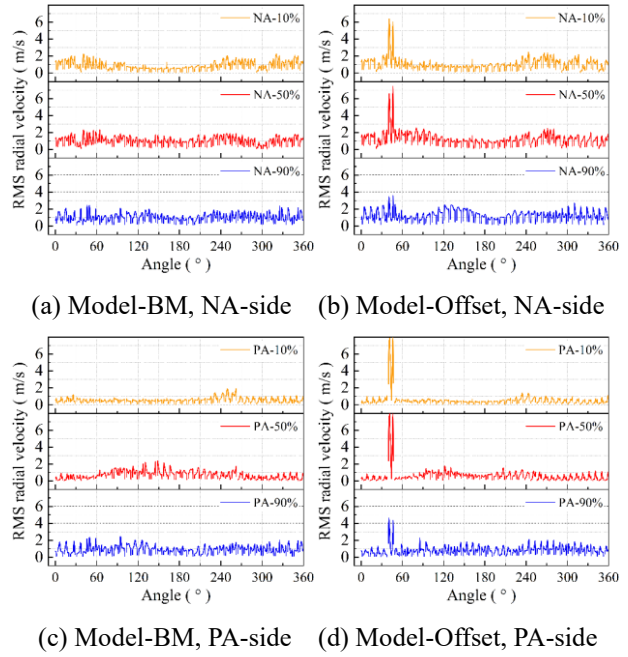


Fig. 23 The distribution of the RMS value of the radial velocity at the middle of the blade passages (R=64mm)

The intensified and weakened fluctuation in the NA-side and PA-side inlet is attributed to varied flow rates, while the leakage flow has less influence. The reduced flow rate in the NA-side results in a flow of high unsteadiness in the central impeller; the flow does not well circulate in the circumferential direction but presents significant radial motion and sweeps over the inlet. On the contrary, the flow in the central impeller still behaves circulating and imposes less perturbation at the inlet. The fluctuation of radial velocity at R=64mm is more uniform than that at the impeller inlet, as seen in Fig. 23; the maximum amplitude is around 2m/s for Model-BM, although there are still local peaks. Since the recirculating vortices are generated in the impeller, the generally uniform fluctuation reflects the persistent but periodically varying vortices. The offset impeller notably affects the fluctuating flow at 40°-50° for both the NA-side and PA-side. The fluctuating amplitude drastically increases in two blade passages; the amplitude is great on the NA/PA-10% and NA/PA-50% cross-sections but is small on the NA/PA-90% cross-section. The occurrence of the local peaks is attributed to the non-confined blade passages that the air could move to the outlet without any obstruction, i.e., the volute surface; thus, the transition between positive and negative radial velocity is great. Moreover, the flow in the axial clearance at 40°-50° experiences a drastic transition between the forward flow and reversed flow, as seen in Fig. 14, another source inducing the peak fluctuation, especially on the NA/PA-10% cross-sections.

The impact of the offset impeller on flow fluctuation at the impeller outlet (R=69mm) is mainly observed on the NA-side, as shown in Fig. 24. Compared with Model-BM, the fluctuating amplitude increases on all cross-sections, especially for the NA-50% and NA-90% cross-sections.

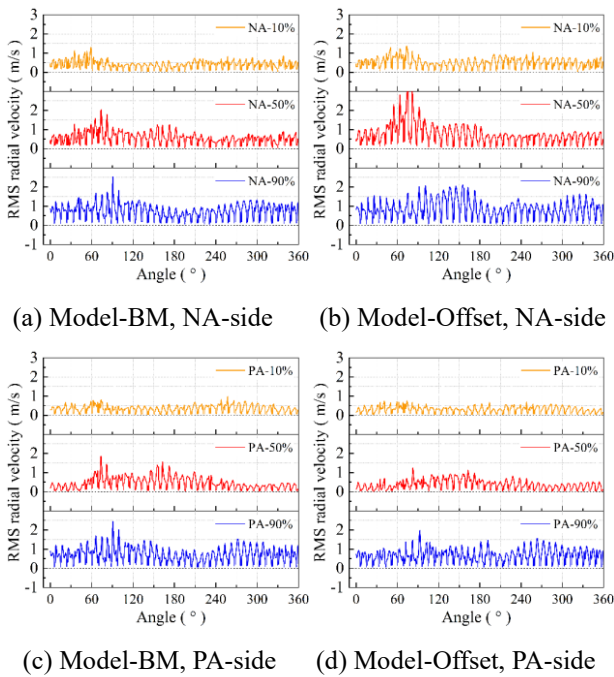


Fig. 24 Distribution of the RMS value of the radial velocity at the outlet of the blade passages ($R=69\text{mm}$)

The rotating impeller energizes the air moving through the blade passages; the kinetic energy increases and the volute confinement is position-dependent. Therefore, the local peaks are observed at 60° - 90° on the NA-10% and NA-50% cross-sections. The offset impeller intensifies and weakens the fluctuation in the NA-side and PA-side due to the varied flow rate.

It is summarized that the flow unsteadiness is noticeable at the inlet ($R=59\text{mm}$) and middle ($R=64\text{mm}$) of the blade passages. The fluctuation gets pronounced as the volute tongue perturbs the flow or is absent from governing the recirculating vortices in the blade passage. The offset impeller intensifies the fluctuation at 40° - 50° in the impeller and at the inlet and outlet of the NA-side impeller. The intensified fluctuation in the NA-side is mainly attributed to the reduced flow rate that the circulating flow periodically sweeps over the blade passages, generating flow entrainment and small-scale secondary vortices at the impeller inlet.

3.7 Asymmetric Flow in the Blade Passages

The volute confines the flow in the impeller, and local reversed flow is formed and is destabilized. The formation, development, and temporal fluctuation of reversed flow are complex and could not be revealed by the velocity recorded by a single monitor. The asymmetric field of instantaneous radial velocity in multiple blade passages around the volute tongue is presented to analyze the flow development. Fig. 25a shows the eight blade passages under investigation, and the expansion view is given in Fig. 25b. The selected blade passages are indexed from #1 to #8. The instantaneous radial velocity field on the $R=59\text{mm}$, 64mm , and 69mm cross-sections is

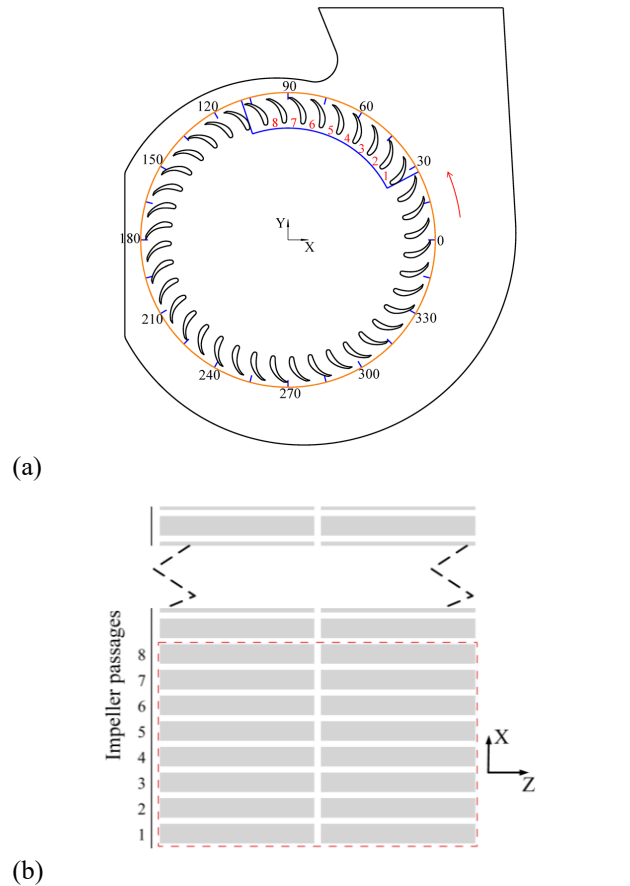


Fig. 25 Notation of the blade passages: (a) the indices of the blade passages; (b) an expansion view of the blade passages

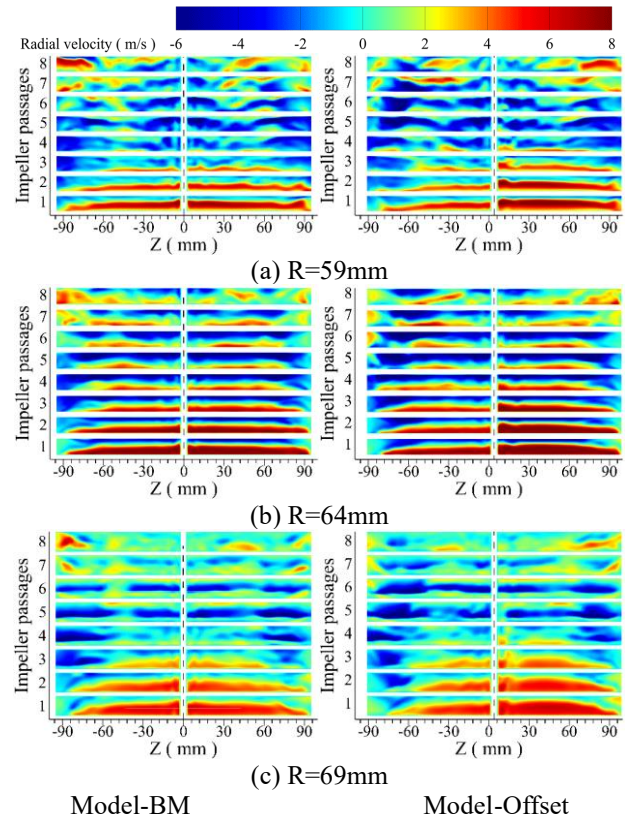


Fig. 26 Field of instantaneous radial velocity on the various constant- R cross-sections

calculated and shown in Fig. 26. The negative radial velocity denotes the reversed flow.

The radial velocity field of Model-BM is generally symmetric about the central disc in blade passages #1-#5 since the flow is not yet confined by the volute tongue surface, and becomes asymmetric in blade passages #6-#8. The asymmetry is pronounced at the inlet ($R=59\text{mm}$) as perturbed by the circulating inflow; it is pretty slight in the middle blade passage ($R=64\text{mm}$) and becomes notable at the impeller outlet ($R=69\text{mm}$), especially near the impeller end rings where the leakage flow in the axial clearance affects.

The reversed flow is formed in all blade passages, although the magnitude and the area differ. It forms on the suction surface at the inlet of blade passage #1, which is far from the volute tongue, although the forward flow dominates; it increases in velocity magnitude and area in blade passages closer to the volute tongue. The blade passages #4 and #5 are almost entirely occupied by the reversed flow, especially in the regions close to the central and the end ring where the magnitude of negative radial velocity reaches maximum. The observation is consistent with the result in Fig. 19, which shows that the reversed flow is more significant on the NA-10% and NA-90% cross-sections than on the NA-50% cross-section. The volute tongue confinement does not impose an evident impact on flow at the impeller inlet; the reversed flow close to the end ring in the blade passages #7 and #8 diminishes, and the forward flow recovers. Referring to Fig. 14, it is concluded that the forward flow is related to the outward leakage flow. In the middle blade passage at $R=64\text{mm}$, the reversed flow reduces in size in blade passages #3-#6, while the magnitude increases due to the local recirculating vortices. The radial velocity field has a much better symmetric pattern in the two halves of the impeller since the flow is confined and driven by the impeller. The quasi-symmetric field persists until the impeller outlet ($R=69\text{mm}$); the radial velocity magnitude decreases as the flow develops in the blade passages.

Compared with Model-BM, the radial velocity field of Model-Offset is asymmetric, and the reversed flow is more significant in area and velocity magnitude in the NA-side impeller, i.e., in blade passages #2-#7 at the inlet ($R=59\text{mm}$) and blade passages #3-#8 at the outlet ($R=69\text{mm}$). The PA-side impeller is occupied mainly by forward flow close to the blade pressure surface, especially in the middle blade passages where persistent recirculating vortices present positive radial velocity.

The radial velocity distribution intuitively reflects the impact of impeller offsetting. The reversed flow is more substantial in the NA-side impeller in the region close to the central disc and the end ring as affected by the radial air motion in the axial clearance. On the contrary, the reversed flow in the PA-side gets weakened in both the magnitude and area, and the velocity magnitude of the forward flow is substantial, showing a better working capability of the PA-side impeller.

3.8 Interactions of Flow in the Volute

The flow in the impeller is confined and separated by the central disc; thus, the flow in the two sides of the impeller does not affect each other. However, the impeller's outflow interacts with the flow in the volute. Fig. 27 denotes the cross-sections at $R=73\text{mm}$, 74.5mm , and 76mm , and

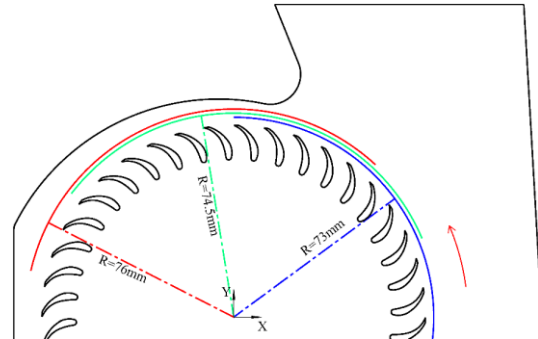


Fig. 27 Definition of the constant-R cross-sections at $R=73\text{mm}$, 74.5mm , and 76mm

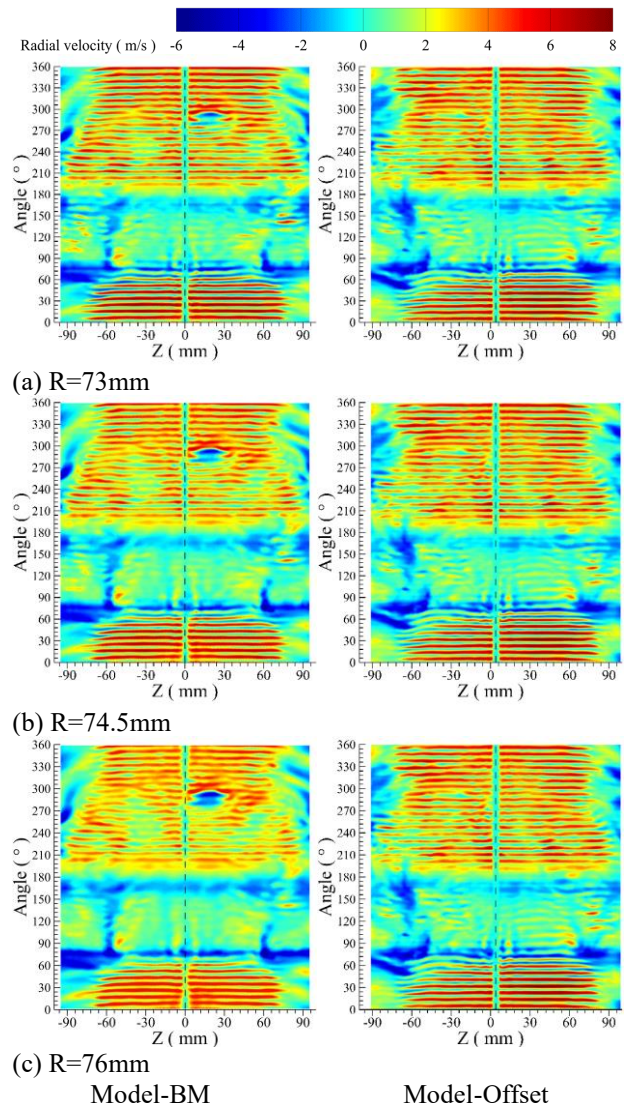


Fig. 28 Instantaneous radial velocity on the various constant-R cross-sections

76mm, and the instantaneous radial velocity distribution is given in Fig. 28 to analyze the evolution of the asymmetric flow as it exits from the impeller.

The forward flow moving toward the volute surface is mainly observed in the blade passages at 0°-60° and 180°-360°, where the gap is large enough to permit the flow development without substantial confinement. It occupies most of the blade passage in the middle and close to the central disc; the velocity magnitude is more significant in blade passages at 0°-60° since the flow is not confined by any surface but directly exits the fan outlet. The weak forward flow with minor positive radial velocity and reversed flow are observed in the blade passages at 60°-180°, and the strong forward flow almost entirely vanishes in this region. The reversed flow is the most pronounced close to the impeller end rings as affected by the leakage flow.

For Model-BM, the radial velocity field does not noticeably vary as the flow develops in the radial direction from R=73mm to R=76mm cross-section. The reversed flow in the blade passages at 60°-90°, which occupies almost the whole blade passage from the end ring to the central disc, increases in magnitude, showing the intense motion back to the impeller as confined by the volute surface. The intensification of reversed flow in this region is much more significant than in other areas, such as the one at 150°-180°, since the radial clearance is larger; thus, the wall confinement is relieved. The asymmetric flow of Model-Offset persists on all cross-sections. Similar to the radial velocity field in the blade passages in Fig. 26, the forward flow is weak in velocity magnitude and area in the NA-side impeller due to the reduced flow rate, and it is more evident as the air moves far from the impeller. The reversed flow around the volute tongue at 60°-90° is intensified throughout the blade passages, with notable expansion close to the NA-side end ring, much larger than that of Model-BM.

The diffusion and interaction of the flow are observed by comparing the radial velocity field at the various radial positions. On the R=73mm cross-section of both models, the velocity field is separated by a virtual central disc. As the air moves in the radial direction, the reversed flow on the two sides starts to merge at 75° and 165° on the R=74.5mm cross-section, and the field of reversed flow at 60°-90° and 150°-180° becomes continuous on the R=76mm cross-section. On the contrary, the merging of the forward flow field on the R=74.5mm cross-section is not noticed, and only the slight merging around 210° on the R=76mm cross-section. This observation implies that the interaction of impeller outflow is dominated by the three-dimensional recirculating vortices, which govern the reversed flow but not the forward flow in the non-blocked blade passages, such as those at 0°-60° and 180°-360°.

3.9 Reversed flow at the Volute Outlet

The varied flow rate and the asymmetric flow in the volute determines the flow at the volute outlet. The Y-velocity, i.e., the velocity component normal to the outlet cross-section, is presented in Fig. 29 using its time-

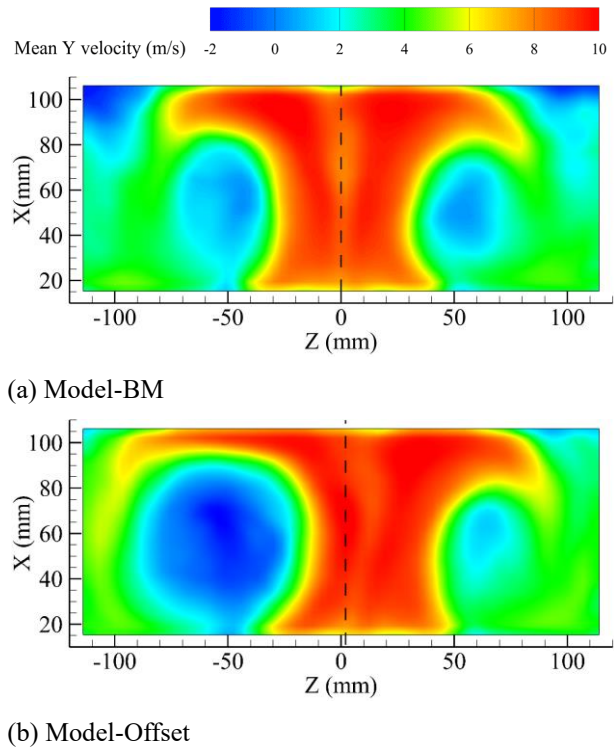


Fig. 29 Distribution of mean Y-velocity on the outflow cross-section of the volute

Table 4 Percentage of the reversed and forward flow at the fan outlet

| Model | Reversed flow | Forward flow |
|--------------|---------------|--------------|
| | By area | |
| Model-BM | 1.83 % | 98.17 % |
| Model-Offset | 8.67 % | 91.33 % |
| | By flow rate | |
| Model-BM | 0.29 % | 99.71 % |
| Model-Offset | 1.35 % | 98.65 % |

averaged value; the positive and negative velocities represent the air exiting from the fan and the air moving backward toward the fan interior, respectively. The velocity field is left-right symmetric about the center of the volute for Model-BM. The forward flow, with positive Y-velocity, occupies most of the cross-section, and the strong reversed flow forms at the top corners and the central region on the two sides of the outlet cross-section. The Y-velocity distribution is consistent with the radial velocity field within and out of the blade passages (Fig. 26 and Fig. 28), that the forward flow dominates around the central disc, and reversed flow forms close to the end rings. For the Model-Offset, the distribution of Y-velocity is notably asymmetric. The forward flow with positive Y-velocity is biased toward the PA-side. The NA-side is occupied by reversed flow in the center and forward flow at the top and center of the cross-section. Although the impeller is offset toward the PA-side by 2mm, the influence is predominant even for the outflow of the fan.

The percentage of reversed flow and forward flow is quantified at the fan outlet by the area and flow rate of the

time-averaged flow. The percentage of reversed and forward flow is listed in Table 4. The reversed flow is generally weak and negligible compared with the forward flow, especially for Model-BM. The offset impeller intensifies the reversed flow; the reversed flow is about 4.7 times that of Model-BM as quantified by the area and flow rate, which is mainly contributed by the strong reversed flow in the NA-side of the fan. The percentage of reversed flow calculated by flow rate is lower than the value by area, implying that the magnitude of reversed flow velocity is much lower than the forward flow.

4. CONCLUSIONS

The transient flow in a double-suction centrifugal fan is numerically investigated using the URANS simulation method to explore the effects of an axially offset impeller on the asymmetric characteristics of flow. The offset impeller reduces the static pressure rise and efficiency by 2.40% and 0.78%, respectively. The mean flow rate reduces by about 5.5% on the NA-side of the fan, while the narrowed clearance on the PA-side of the fan partially blocks the leakage and increases the local flow rate. The offset impeller increases the mean static pressure and reduces the mean axial velocity in the NA-side collector, and the opposite influence applies to the PA-side collector.

The fluid inertia and the radial pressure gradient determine the leakage flow in the axial clearance. The outward motion of leakage flow is predominant in the enlarged clearance on the NA-side of the Model-Offset, while the narrowed clearance on the PA-side partially blocks it. The volute tongue confinement generates persistent inward-moving air.

The offset impeller affects the flow in the impeller in the region close to the collector, and the impact is more pronounced for the NA-side. The volute confinement produces persistent reversed flow around the volute tongue. The flow unsteadiness is noticeable at the inlet and middle of the blade passages and is pronounced by the volute tongue perturbation or the absent governing of the recirculating vortices. The intensified velocity fluctuation on the NA-side is due to the reduced flow rate. The circulating flow periodically sweeps over the blade passages, generating flow entrainment and small-scale secondary vortices at the inlet. As the flow develops in the radial direction, the reversed flow in the blade passages gets weakened on the PA-side but is not apparent on the NA-side impeller. The reversed flow is still significant as the flow exits the NA-side impeller, especially close to the impeller end ring and at 60°-90° due to the volute tongue confinement. The impact of impeller offsetting on the flow persists till the fan outlet. The reversed outflow is more substantial for Model-Offset, and most reversed flow are in the central region of the NA-side fan.

It is summarized that the impeller offsetting generates noticeable asymmetric flow in the fan. The asymmetric and temporally fluctuating flow imposes unbalanced forces on the impeller and volute, presenting different ventilation capabilities at the two inlets. The conclusions of this study could be referred to in possible applications

where the impeller offsetting, either axially or in other manners (Chen et al., 2022, 2024), is considered in a double-suction centrifugal turbomachine.

ACKNOWLEDGEMENTS

The work was supported by Natural Science Foundation of China (52176047).

CONFLICT OF INTEREST

The authors have no conflicts to disclose.

AUTHOR CONTRIBUTION

Ruifeng Liu: Data curation, Formal analysis, Investigation, Methodology, Software, Writing-original draft. **Hui Yang:** Formal analysis, supervision. **Yikun Wei:** Formal analysis, supervision. **Wei Zhang:** Conceptualization, Formal analysis, Funding acquisition, Investigation, Project administration, Resources, Supervision, Writing-review & editing.

REFERENCES

- Chen, Z. Y., He, H., Yang, H., Wei, Y. K., & Zhang, W. (2024). Asymmetric flow in a double-suction centrifugal fan induced by an inclined impeller. *Physics of Fluids*, *36*, 017113. <https://doi.org/10.1063/5.0178927>
- Chen, Z. Y., Yang, H., Wei, Y. K., He, H. J., Zhang, C. Y., Nie, T. H., Yu, P. Q., & Zhang, W. (2022). Effect of a radially offset impeller on the unsteady characteristics of internal flow in a double-suction centrifugal fan. *Processes*, *10*, 1604. <http://dx.doi.org/10.3390/PR10081604>
- Deng, Q. F., Pei, J., Wang, W. J., & Sun, J. (2023). Investigation of energy dissipation mechanism and the influence of vortical structures in a high-power double-suction centrifugal pump. *Physics of Fluids*, *35*, 075147. <https://doi.org/10.1063/5.0157770>
- Ding, J., Du, X., Zhang, L. X., Jiang, T., & Wang, S. T. (2012). Investigation of the effect of volute openness on aerodynamic characteristics of a centrifugal fan. *Chinese Journal of Turbomachinery*, *5*, 22–26. (in Chinese). <http://dx.doi.org/10.3969/j.issn.1006-8155.2012.05.005>
- Gangipamula, R., Ranjan, P., & Patil, R. S. (2022). Study of rotor-stator interaction phenomenon in a double-suction centrifugal pump with impeller vane trailing edge as a design parameter. *Physics of Fluids*, *34*, 095131. <https://doi.org/10.1063/5.0105576>
- González, J., Parrondo, J., Santolaria, C., & Blanco, E. (2006). Steady and unsteady radial forces for a centrifugal pump with impeller to tongue gap variation. *Journal of Fluids Engineering*, *128*, 454-462. <https://doi.org/10.1115/1.2173294>

- He, C., Han, W., Li, R., Dong, Y. & Zhang, Y. (2025) Multi-objective optimization and performance analysis of the splitter blades in a multiphase pump. *International Journal of Fluid Engineering*, 2, 013501. <https://doi.org/10.1063/5.0229988>
- Jin, J. M., Jung, K. J., Kim, Y. H., & Kim, Y. J. (2020). Effects of gap between impeller and volute tongue on pressure fluctuation in double-suction pump. *Journal of Mechanical Science and Technology*, 34, 4897-4903. <http://doi.org/10.1007/s12206-020-2102-3>
- Lee, Y. T. (2010). Impact of fan gap flow on the centrifugal impeller aerodynamics. *Journal of Fluids Engineering*, 132, 091103. <https://doi.org/10.1115/1.4002450>
- Lei, L., Wang, T., Qiu, B., Yu, H., Liu, Y. Q., & Dong, Y. C. (2024). The influence of ring clearance on the performance of a double-suction centrifugal pump. *Physics of Fluids*, 36, 025133. <https://doi.org/10.1063/5.0188087>
- Li, W. (2025) Performance of vortex pump in CFD simulations with rough walls. *International Journal of Fluid Engineering*, 2, 013902. <https://doi.org/10.1063/5.0237732>
- Li, Z. H., Ye, X. X., & Wei, Y. K. (2020). Investigation on vortex characteristics of a multiblade centrifugal fan near volute outlet region. *Processes*, 8, 1240. <https://doi.org/10.3390/pr8101240>
- Lilly, K. (1992). A proposed modification of the Germano subgrid-scale closure method. *Physics of Fluids*, 4, 633–635. <https://doi.org/10.1063/1.858280>
- Liu, H., Jiang, B. Y., Wang, J., Yang, X. P., & Xiao, Q. H. (2021). Numerical and experimental investigations on non-axisymmetric D-type inlet nozzle for a squirrel-cage fan. *Engineering Applications of Computational Fluid Mechanics*, 15, 363–376. <https://doi.org/10.1080/19942060.2021.1883115>
- Liu, X. M., Dang, Q., & Xi, G. (2008). Performance improvement of centrifugal fan by using CFD. *Engineering Applications of Computational Fluid Mechanics*, 2, 130–140. <https://doi.org/10.1080/19942060.2008.11015216>
- Liu, Z., Wang, Z., Du, S., Yang, H., Wei, Y., & Zhang, W. (2024). Orthogonal optimization design of a Sirocco fan and numerical analysis on the internal flow characteristics, *Journal of Power and Energy*, 238, 90-110. <https://doi.org/10.1177/09576509231195120>
- Lu, J., Qian, L., Liu, X., & Choi, Y. (2024) Characterization of energy loss in jet mechanism of a Pelton turbine. *International Journal of Fluid Engineering*, 1, 033502. <https://doi.org/10.1063/5.0209402>
- Lv, Y. K., Zhang, B., & Cheng, B. (2014). The optimal research on impeller central location of centrifugal fan. *Applied Mechanics and Materials*, 668-669, 729-732. <https://doi.org/10.4028/www.scientific.net/AMM.668-669.729>
- Madhresh, N., Karanth, K. V., & Sharma, N. Y. (2018). Effect of innovative circular shroud fences on a centrifugal fan for augmented performance: A numerical analysis. *Journal of Mechanical Science and Technology*, 32, 185–197. <https://doi.org/10.1007/s12206-017-1220-z>
- Morinushi, K. (1987). The influence of geometric parameters on F. C. centrifugal fan noise. *Journal of Vibration and Acoustics*, 109, 227-234. <https://doi.org/10.1115/1.3269425>
- Myung, H. J., & Baek, J. H. (1999). Mean velocity characteristics behind a forward-swept axial-flow fan. *JSME International Journal Series B*, 42, 476–488. <https://doi.org/10.1299/jsmeb.42.476>
- Okauchi, H., Suzuka, T., Sakai, T., & Whitfield, A. (2002). *The effect of volute tongue and passage configuration on the performance of centrifugal fan*. International Compressor Engineering Conference, Paper No. 1502.
- Pan, D., Whitfield, A., & Wilson, M. (1999). Design considerations for the volutes of centrifugal fans and compressors. *Proceedings of the Institution of Mechanical Engineers, Part C: Journal of Mechanical Engineering Science*, 213, 401–410. <https://doi.org/10.1243/0954406991522356>
- Patil, S. R., Chavan, S. T., Jadhav, N. S., & Vadgeri, S. S. (2018). Effect of volute tongue clearance variation on performance of centrifugal blower by numerical and experimental analysis. *Materials Today: Proceedings*, 5, 3883-3894. <https://doi.org/10.1016/j.matpr.2017.11.643>
- Rui, X. C., Lin, L. M., Wang, J. K., Ye, X. X., He, H. J., Zhang, W., & Zhu, Z. C. (2020). Experimental and comparative RANS/URANS investigations on the effect of radius of volute tongue on the aerodynamics and aeroacoustics of a Sirocco fan. *Processes*, 8, 1442. <https://doi.org/10.3390/pr8111442>
- Samarbakhsh, S., & Alinejad, J. (2011). *Experimental and numerical analysis of eight different volutes with the same impeller in a squirrel-cage fan*. 2nd European Conference of Control and Mechanical Engineering, 198-203.
- Smagorinsky, J. (1963). General circulation experiments with the primitive equations. I. The basic experiment. *Monthly Weather Review*, 91, 99–164. [https://doi.org/10.1175/1520-0493\(1963\)091%3C0099:GCEWTP%3E2.3.CO;2](https://doi.org/10.1175/1520-0493(1963)091%3C0099:GCEWTP%3E2.3.CO;2)
- Sonawat, A., Kim, S., Ma, S. B., Kim, S.-J., Lee, J. B., Yu, M. S., & Kim, J. H. (2022). Investigation of unsteady pressure fluctuations and methods for its suppression for a double suction centrifugal pump. *Energy*, 252, 124020. <https://doi.org/10.1016/j.energy.2022.124020>
- Song, Y., Fan, H. G., Zhang, W., & Xie, Z. F. (2019). Flow characteristics in volute of a double-suction

- centrifugal pump with different impeller arrangements. *Energies*, 12, 669. <https://doi.org/10.3390/en12040669>
- Sun, L., An, C., Wang, N., Zhe, C., Wang, L., He, S., & Gao, M. (2021). Effect of the rotor blade installation angle on the structure-borne noise generated by adjustable-blade axial-flow fans, *Physics of Fluids*, 33, 095107. <https://doi.org/10.1063/5.0065356>
- Versteeg, H. K., & Malalasekera, W. (2007). *An Introduction to Computational Fluid Dynamics*. Pearson Education, Essex, UK.
- Wu, L.N., Liu, X. M., & Wang, M. H. (2020). Effects of bionic volute tongue on aerodynamic performance and noise characteristics of centrifugal fan used in the air-conditioner. *Journal of Bionic Engineering*, 17, 780-792. <https://doi.org/10.1007/s42235-020-0067-7>
- Yang, X., Chen, W. M., Yuan, M. J., Wen, X. F., & He, M. (2011). Experimental study on the effect of relative impeller to volute position on the performance of multiblade centrifugal fan. *Fluid Machinery*, 39, 1-5. (in Chinese) <http://dx.doi.org/10.3969/j.issn.1005-0329.2011.07.001>
- Ye, J. J., Liu, W. W., Duan, P., Huang, X. Y., Shao, J. D., & Zhang, Y. (2018). Investigation of the performance and flow behaviors of the multi-blade centrifugal fan based on computer simulation technology. *Wireless Personal Communications*, 103, 563–574. <https://doi.org/10.1007/s11277-018-5461-7>
- Younsi, M., Bakir, F., Kouidri, S., & Rey, R. (2007). Numerical and experimental study of unsteady flow in a centrifugal fan. *Journal of Power and Energy*, 221, 1025-1036. <https://doi.org/10.1243/09576509JPE445>
- Zhang, J. H., Chu, W. L., Zhang, H. G., Wu, Y. H., & Dong, X. J. (2016). Numerical and experimental investigations of the unsteady aerodynamics and aero-acoustics characteristics of a backward curved blade centrifugal fan. *Applied Acoustics*, 110, 256-267. <https://doi.org/10.1016/j.apacoust.2016.03.012>
- Zhou, S. Q., Wang, M., Li, Z. Y., & Zhang, S. C. (2018). Influence of volute retrofit design on performance of multiblade centrifugal fan. *Transactions of the Chinese Society of Agricultural Machinery*, 49, 180-186. (in Chinese) <http://dx.doi.org/10.6041/j.issn.1000-1298.2018.10.020>